International Journal of Engineering Technologies and Management Research

IJETMR

A Knowledge Repository

EXPERIMENTAL AND NUMERICAL STUDIES ON MULTI-BOLT DOUBLE COVER BUTT JOINTED GLASS FIBRE REINFORCED COMPOSITE LAMINATES WITH ALUMINIUM BUTT STRAPS

S. S. Subramanya Sastry [*1]**, Sivanagaraju Reddy** [2]**, K. Naresh Babu** [3]
[1] DGM, A & D, Cyient Limited, India
[2] M.Tech Student, JNTU, Kakinada 500032, India
[3] Assistant Professor, Chebrolu Engineering College, Department of Mechanical Engineering JNTU (K), Andhra Pradesh, 522212, India

Abstract:

Numerical and experimental studies on multi-bolt double cover butt jointed glass fibre reinforced composite laminates with Aluminium butt straps (size 270 x 72 x 3/4/5 mm) subjected to a tensile load are presented. Experiments were conducted using the assembled specimens in Instron testing machine under uniaxial load. The test specimens exhibited bearing failure of the laminate at all bolt points followed by net tension failure along the line of bolts close to the grips. Investigation are conducted to study the effects of material composition, consistency of fabrication, bearing-bypass interaction / damage onset, specimen thickness on the stress-strain behaviour of the specimen, load distribution in bolts, types of fit and friction, material anisotropy and contact condition under bolt preload. Influence of these parameters on the contact stresses around the bolt and stresses in the butt straps are discussed. Finite element analysis was carried out using ANSYS for various parameters and results were compared with test data.

Nomenclature

a, b – Semi major (or radius) and minor axis of the bolt hole, mm

A_{ij} – Coefficients of extensional stiffness matrix of the laminate of the bolted joint, N/mm

A_{11}^{-1} - Inverted coefficient of axial stiffness matrix of the laminate of the specimen, mm/N

d – Major (largest) diameter of the bolt, mm

d_m – Mean diameter of the bolt thread, mm

d_c – Mean Collar diameter, mm

D – Diameter of the bolt hole, mm

E, E_1, E_2, E_3 – Young's Modulus in the three mutually perpendicular directions, MPa

G_{12}, G_{23}, G_{31} – Shear Modulus in the three mutually perpendicular planes, Mpa

E_x – Longitudinal modulus of the laminate of the specimen, MPa

E_s - Secant modulus of the material in the plastic state, MPa

$(E_s)_\infty$ - Secant modulus of the material in the plastic state at r = ∞, MPa

FEA – Finite Element Analysis

G – is function of the E_s / $(E_s)_\infty$ at the point stress calculation (r,θ)

H – Width of the composite plate containing the bolt hole, mm

h – Thickness of the composite laminate, mm ($\sum_{i=1}^{N} t_i$)

K – Torque Coefficient for bolt preload

---

l – Lead, distance moved by the nut parallel to the screw axis in one turn of the nut, mm

L – Distance between the center of the bolt hole and section at which specimen displacement is measured, mm

$LVDT$ – Linear Variable Differential Transformer

N – Number of layers in the laminate

NT – Net Tension

P – Applied load on the bolted joint, N

r – Distance from bolt hole center at which stresses are calculated, mm

TRB – Tension Reacted Bearing

t_i – Thickness of each lamina in the laminate, mm

X – Distance between the bottom of the bolt hole and section at which displacement from the finite element model of the specimen is computed (represents the extent of zero strain part), mm

λ – Lead Angle, degrees

α – Thread Angle, degrees

$\mu_{12}, \mu_{23}, \mu_{31}$ - Poisson's Ratios in three mutually perpendicular planes

μ – Coefficient of thread friction

μ_c - Coefficient of collar friction

μ_c - Coefficient of collar friction

$\delta_{corrected}$ – Corrected deformation of the bolt hole, mm

δ_L – Displacement of test specimen read by LVDT, mm

δ_{Hole} – Deformation of the bolt hole, mm

σ / σ_∞ – Applied stress at the loading end of the specimen, N/sq.mm

δ_1 – Actual hole deformation that has to be measured to report a correct bearing strain

Φ – Transverse compressive crack angle in the matrix, degree

Keywords: Experimental; Numerical Studies; Reinforced; Composite.

1. Introduction

Due to high strength to weight and stiffness to weight ratio, composite laminates have been extensively used in aircraft and space vehicles. In airframe construction to achieve the size and shape of the vehicle, three types of composite joints namely mechanically fastened joints, bonded joints and hybrid joints are used. Mechanically fastened joints offer better advantage over the other two in terms of disassembly of the structure for inspection and repair. In mechanically fastened configuration, multiple bolts and rivets are used to connect various structural parts and transfer loads among them. The multi-bolted joints are affected by different joint parameters and are subject to bypass versus bearing loading, with each row of fasteners removing some of the load (bearing load) whilst the remaining load is taken up by the following fasteners (bypass load) [1–4]. The ratio of the bypass load versus the bearing load has been shown to affect the joint strength and the failure mode [3]. The variations in bolt-hole clearance in the joints are found to increase

the contact stress distribution under the bolt and thereby reduce the bearing load on the laminate [5-12]. Interference fit is shown to be beneficial for all pin loaded joint configurations. Progressive damage analysis proved very effective to predict the successive failure of the plies of the laminate. Missing fasteners are understood cause significant losses in load carrying capacity of the joint. Fasteners in the vicinity of the empty hole together with bolts located in the same column (line of bolts parallel to the applied load)as the empty hole, experience significant increase in load. The account of non-linear response of the joint results in a less conservative load distribution at ultimate failure load of a joint. Bearing failure is outlined as a process of compressive damage accumulation and is divided into the following four stages namely damage onset, damage growth, local fracture and structural failure [11 – 25].

The studies conducted in the literature pertain to a single or multiple bolted joints either simple or hybrid are limited to lap joints. Loading axis of members of a lap joint are offset from each other. Hence the load passing through the connected plates is eccentric. This type of loading results in an uneven stress distribution in the members. This leads to bending of the joints and direct shear loading on the bolts eventually joints failure occurs at lower loads.

Butt joints are used to avoid these types of difficulties and they also carry higher loads. Two types of butt joints are used in practice. They are the single and double cover plate butt joints. Single cover butt joints are also subjected to eccentric loads and bending of the joints. In a double cover plate butt joint the shear load is shared between two cover plates. Also, because of the absence of eccentricity the joint doesn't experience any local bending.

In this paper experimental and numerical studies on double cover butt joints are presented. Experiments are conducted on an Aluminium-GFRP double cover butt joint. Test specimens exhibited bearing failure at all bolt points followed by net tension failure. Three-dimensional nonlinear stress analysis of the specimens is performed using ANSYS software and the results of the simulation are compared with the experimental observations.

2. Specimen Description and Test Set Up

Three types of specimens of nominal thickness 3 to 5 mm were fabricated using 6781 S2 glass fabric with LY556 epoxy resin, HY905 hardener, DY040 plasticizer and DY062 accelerator. The butt straps were fabricated using 5 mm thick AA6061-T4. Quasi-isotropic layup was used for fabricating specimens. Five specimens each were fabricated with nomenclature T3D6E3W6, T4D6E3W6 and T5D6E3W6. T3D6E3W6 represents a specimen with a nominal thickness of 3 mm; pitch of the two bolts is 6D; edge distance is 3D and the half width of the specimen is 6D where D (6 mm) is the nominal diameter of the bolt.

Tests were conducted at room temperature and moisture. The specimens were prepared by the matched die compression molding process (mould material is EN8 steel) shown in Figure 1.
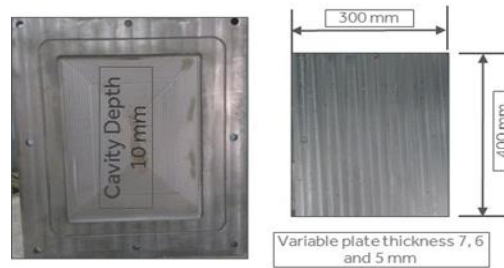
Figure 1: Matched die mold used to prepare specimens

The mean thickness of the laminates for T3D6E3W6 specimen was 3.328 mm, T4D6E3W6 specimen was 4.502 mm and T5D6E3W6 specimen was 5.672 mm. Test specimen is assembled with the help of two FRP plates of sizes (72 * 135 mm) and two Aluminum butt straps (72 * 145 mm). Drilling of 8 holes onto the specimen assembly is carried out with the help of jig. M6 Unbrako bolts were tightened to a torque of 2.2 N-m. For each specimen category, 5 specimens were prepared and the dimensions were averaged for developing the finite element model. The average fiber volume fraction obtained for all the specimens 63% (63 % fiber and 37% matrix) and average density of GFRP was 1.7 g/cc.

The specimens were tested in an Instron testing machine (Figure. 2, NAL, Bangalore) with cross head speed of 2 mm / minute as per ASTM D 5961/D 5961M – 08 per Procedure A (bolts under double shear, tension). Dimensions of the specimen are shown in Figure. 3. The washer thickness is 1.5 mm, outer diameter is 12 mm and inner diameter is 6.5 mm. One steel washer each is used on the head and nut side for uniform distribution of pressure due to torque. The numerical studies are carried out for snug fit, interference fit (0.16 mm) and clearance 0.079 mm.


Figure 2: Specimen mounted on INSTRON testing machine
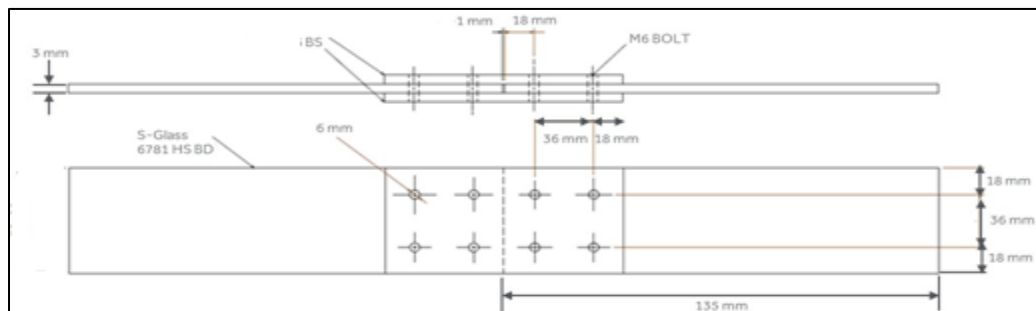
Figure 3: Double lap butt joint of GFRP laminates with AA 6061-T4 butt straps for a quasi-isotropic layup (Torque = 2.2 N-m)

3. Numerical Model

A three dimensional finite element model (Figure. 4) of the butt joint was developed using ANSYS Workbench code considering the non-linear stress computations accounting for the composite material and contact behaviour. A characteristic curve with Roc = 2.4 mm and Rot = 1.2 mm [18] was incorporated into the model. The onset of failure is predicted using Hashin failure criteria around the characteristic curve. The mechanical properties of the materials used for the butt joint is shown in Table 1 and 2 [26].

The preload generated due to bolt torqueing is given by

$$T = \left[\left(\frac{d_m}{2d} \right) * \left(\frac{\tan \lambda + \mu \sec \alpha}{1 - \mu \tan \lambda \sec \alpha} \right) + 0.625 \, \mu_c \right] * F_i * d \tag{1}$$

$$T = K * Fi * d \tag{2}$$

Torque coefficient K = 0.3 is used in the present study [25].
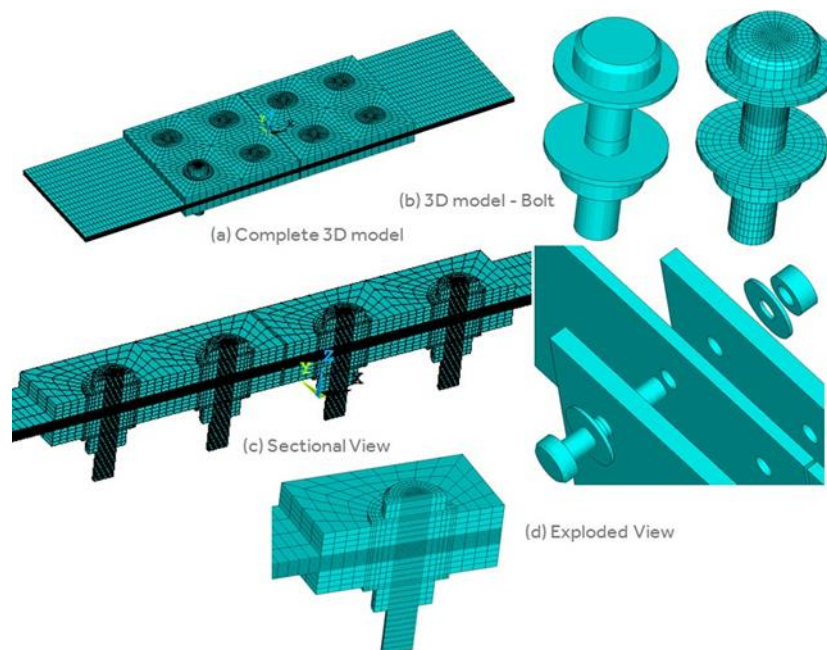

Figure 4: Three dimensional finite element model of double lap butt joint of GFRP laminates with AA 6061-T4butt straps for a quasi-isotropic layup (Torque = 2.2 N-m)

Table 1: Elastic properties of glass epoxy prepreg 6781 8HS S2 fabric

Sl. No.	Property	6781 8HS S2 BD Prepreg
1	Young's Modulus (E_1, MPa)	29095.88
2	Young's Modulus (E_2, MPa)	27889.29
3	Young's Modulus (E3, MPa)	27889.29
4	Shear Modulus (G12, MPa)	3792.12
5	Shear Modulus (G23, MPa)	3792.12

6	Shear Modulus (G31, MPa)	3792.12
7	Poisson's Ratio (μ_{12})	0.14
8	Poisson's Ratio (μ_{23})	0.14
9	Poisson's Ratio (μ_{31})	0.14
10	Fiber strength (longitudinal X_t, MPa)	551.58
11	Fiber strength (longitudinal X_c, MPa)	558.47
12	Fiber strength (Transverse Y_t, MPa)	544.68
13	Fiber strength (Transverse Y_c, MPa)	461.94
14	Fiber strength (In plane S_{12}, MPa)	63.15
15	Fiber strength (Out of plane S_{23}, MPa)	174.05#
16	Fiber strength (Out of plane S_{31}, MPa)	63.15

calculated per [27] as explained below

S23 is calculated from transverse compressive strength using the equation

$$S_{23} = \frac{Y_c}{\left(2 * \tan(\varphi)\right)} \tag{3}$$

φ is the transverse compressive crack angle and is usually taken as 530.

Table 2: Properties of the AA6061-T4 butt straps [28] and HSS bolt [29]

Sl. No.	Property	HSS Bolt	Butt Strap
1	Young's Modulus, E	210000	68258.11
2	Poisson's Ratio	0.31	0.33

3.1. Finite Element Modeling

Contact interactions were modelled using 'surface-to-surface' based contact considering the Augmented Lagrange method. Contact interactions were defined between all the solids in entire model; the composite plate was in contact with aluminium plates and bolt shank and aluminium plate was in contact with washer and bolt shank. Two friction coefficients were used for parametric studies viz., 0.0 [5] and 0.1 [9]. The loading was divided into two steps. In the first step, free ends of composite plates were clamped (UX=UY=UZ=0) and tightening torque was applied as a bolt preload. The bolt preload was implemented in the finite element model by introducing a pre-tension condition. This pre-tensioning is simulated in ANSYS by adding a "cutting section" in the bolt shank and subjecting it to a normal load.
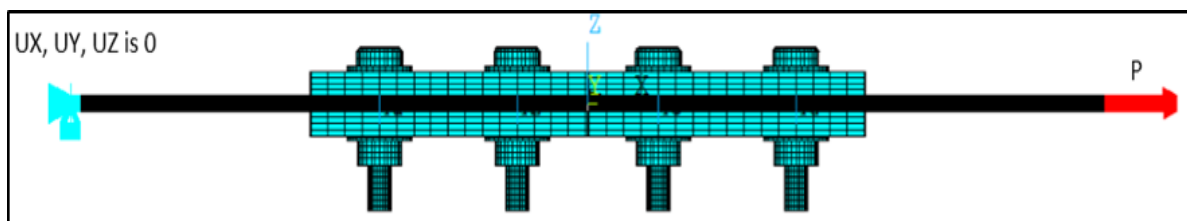

Figure 5: Load and boundary conditions of Double lap butt joint of GFRP laminates with AA 6061-T4 butt straps model for a quasi-isotropic layup (Torque = 2.2 N-m)

This finite element model was developed to analyse the force displacement relationship along with identification of failure modes. The characteristic element size in the FE mesh was 2.5 mm. Mesh density was carefully regulated around the bolt hole and characteristic curve so as to predict the failure along the curve. Total of 144256 SOLID185–3-D 8-Node Solid element with selected full integration were used with one element per layer. Composite laminates were modelled using 49280 elements, butt straps were modelled using 20736 elements and 74240 elements were used to model the bolt and the nuts.

4. Results and Discussions

The results are presented under various sections below.

4.1. Study of Material Composition and Elastic Constants of the Specimens

Material composition and basic specimen laminate elastic properties are shown in Table 3.

Table 3: Material composition and laminate elastic constants

Layers	Specimen	% of 0^0 layers	% of 90^0 layers	% of $\pm45^0$ layers	% Fibers (V_f)	% Matrix (V_m)
14	T3D6E3W6	28.57	28.57	42.86	63.43	36.61
18	T4D6E3W6	33.33	28.57	57.14	63.77	36.22
22	T5D6E3W6	27.27	27.27	45.45	NA	NA

Specimen	E_x, CLT	E_y, CLT	G_{xy}, CLT	v_{xy}, CLT
T3D6E3W6	22937.8	22937.8	7545.83	0.31
T4D6E3W6	22762	22638.6	7684.97	0.31
T5D6E3W6	22547.7	22547.7	7773.40	0.31

Specimen laminate elastic properties are given by equations [32]

Effective in-plane longitudinal modulus

$$E_x = \left(\frac{1.0}{h * A_{11}^{-1}} \right) \tag{4}$$

Effective in-plane transverse modulus

$$G_{xy} = \left(\frac{1.0}{h * A_{66}^{-1}} \right) \tag{5}$$

Effective in-plane shear modulus

$$G_{xy} = \left(\frac{1.0}{h * A_{66}^{-1}} \right) \tag{6}$$

Effective in-plane Poisson's ratio

$$v_{xy} = \left(-\frac{A_{12}^{-1}}{A_{11}^{-1}} \right) \tag{7}$$

4.2. Study of Consistency of Fabrication Procedure of Specimens

The specimens' width, diameter and edge distance were measured at various points on their geometry and a statistical analysis was carried out to predict standard deviation and coefficient of variation of these dimensions. The results are presented in Table 4. It is observed that the standard deviation and coefficient of variation are low which means the various (W/D), (E/D) and (D/t) ratios measured are accurate and precise. This establishes the fact that the specimens were fabricated using consistent procedure.

Table 4: Statistical analysis of the specimen parameters

Description	Specimen	Mean	Standard Deviation	Coefficient of Variation
Actual (Width/Diameter) ratio	T3D6E3W6	12.5035	0.2473	1.9777
	T4D6E3W6	12.4841	0.1432	1.1468
	T5D6E3W6	12.4176	0.0831	0.6688
Actual Edge Distance to Diameter Ratio	T3D6E3W6	3.1183	0.0773	2.4804
	T4D6E3W6	3.1249	0.0516	1.6522
	T5D6E3W6	3.1086	0.0339	1.0913
Actual (Diameter/ Thickness) Ratio	T3D6E3W6	1.6833	0.0432	2.5643
	T4D6E3W6	1.2775	0.0208	1.6281
	T5D6E3W6	1.0144	0.0107	1.0553

4.3. Study of Prediction of Damage Onset and Bearing Bypass Stress Computation

Results of the bearing-bypass computations are presented in Figure. 6 and 7; Table 5 and 6. The stresses σb (bearing stress) and σbyp (bypass stress) correspond to the onset of damage or the first ply failure [6]. The bearing stress, net section bypass stress and bearing bypass ratio are defined as

$$Bearing\,Stress, S_b = \frac{P_{br}}{D*h} \tag{8}$$

$$Nominal\,Net\,Section\,Bypass\,Stress, S_{np} = \frac{P_{byp}}{(w-d)*h} \tag{9}$$

$$Bearing-Bearing\,Bypass\,ratio, \beta = \frac{S_b}{S_{np}} \tag{10}$$

Bearing Bypass diagrams are developed in Figure 6 and 7, where two types of failure modes are identified viz., Net Tension (NT) indicates the net tension damage and the bearing failure. The tests carried out (for 5 specimens in each group) up to the failure load resulted in net tension failure of the specimen as shown in Figure 8. Bearing damage onset in the specimen is indicated by the

Tension Reacted Bearing (TRB). This damage is observed at the line joining bolts 1 and 2 closer to the grip side of the specimen as shown in Figure 8.

From Tables 5 and 6, Net Tension (NT) mode of damage (bearing-bypass ratio, β = 0 to 0.42, including 4 holes) is represented by a straight line and shows a linear interaction [1]. Linearity is taken to be consisting of two components one due to bearing and a second component due to bypass stress [6]. The   'bearing cut-off line is represented by a thick horizontal line ($\beta = \infty$, Figure 6 and 7). These two lines through the data define the onset damage strength (first ply failure) for different combinations of bearing and bypass loading in tension. Since no tests are done by us in compression loading, bearing-bypass diagrams are not reported in this paper.
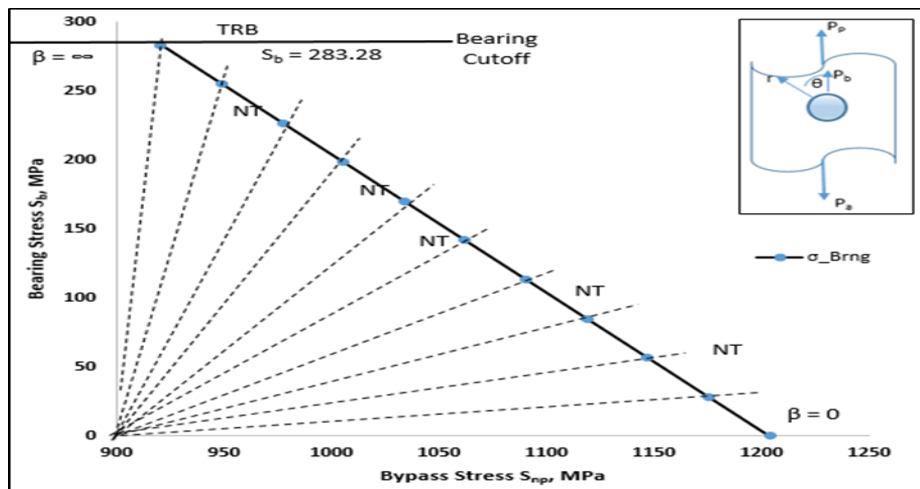
Figure 6: Bearing Bypass diagram for damage onset strength section passing through bolt holes 1 and 2
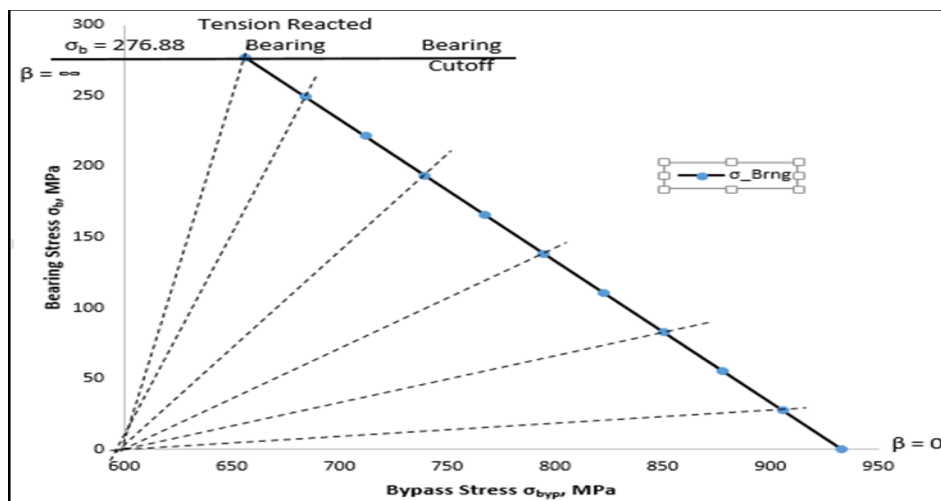
Figure 7: Bearing Bypass diagram for damage onset strength section passing through bolt holes 3 and 4

Figure 8: Net Tension Failure of specimen along the line joining bolts 1 and 2

Table 5: Damage onset data

Damage Onset Data Bolts 1 and 2				
Loading	Bearing-Bypass Ratio, β	Damage Onset Strength		Damage Onset Mode
		σ_b MPa	σ_{byp} MPa	
Tension	0.00	0.00	1203.81	Net tension
	0.02	28.33	1175.49	Net tension
	0.05	56.66	1147.16	Net tension
	0.08	84.99	1118.83	Net tension
	0.10	113.32	1090.50	Net tension
	0.13	141.64	1062.17	Net tension
	0.16	169.97	1033.84	Net tension
	0.20	198.30	1005.51	Net tension
	0.23	226.63	977.18	Net tension
	0.27	254.96	948.85	Net tension
	0.31	283.29	920.52	Net tension
	Infinity	283.29	0.00	Tension Reacted Bearing

Table 6: Damage onset data

Damage Onset Data Bolts 3 and 4				
Loading	Bearing-Bypass Ratio, β	Damage Onset Strength		Damage Onset Mode
		σ_b MPa	σ_{byp} MPa	
Tension	0.00	0.00	933.33	Net tension
	0.03	27.69	905.64	Net tension
	0.06	55.38	877.95	Net tension
	0.10	83.07	850.26	Net tension
	0.13	110.76	822.57	Net tension
	0.17	138.44	794.88	Net tension
	0.22	166.13	767.19	Net tension
	0.26	193.82	739.51	Net tension
	0.31	221.51	711.82	Net tension
	0.36	249.20	684.13	Net tension
	0.42	276.89	656.44	Net tension
	Infinity	283.29	0.00	Tension Reacted Bearing

4.4. Study of Effect of Thickness on The Stiffness of The Specimen

The ultimate load of each specimen were obtained from the load versus cross head displacement readings. The cross head displacement was plotted against the applied load as shown in Figure 9. The specimens have shown a nonlinear behaviour. The three curves have a small initial non-linearity (possibly due to varying contact arc between the bolt and the specimen) but they develop a nearly linear response gradually. As the load increases, the curves develop a second non-linear behaviour. This indicates the development of a damage at the bolt holes [32]. It clear from the three curves in Figure 10 that the joints constructed from thicker laminates are stiffer and they transmit higher loads than joints with thinner laminates (in agreement with, [17]). In terms of energy absorption for a butt joint, it is clear from load versus cross head displacement readings that thick joints show higher specimen displacement than the thin specimens in contrast to a lap joint [17]. This is due to the fact that in a double lap butt joint the load is symmetrical with respect to the mid plane of the joint and hence all the components of the joint are equally symmetrically loaded in contrast to a lap joint in which a there is a possibility of a small bending moment due to the offset of the center line of the laminates.
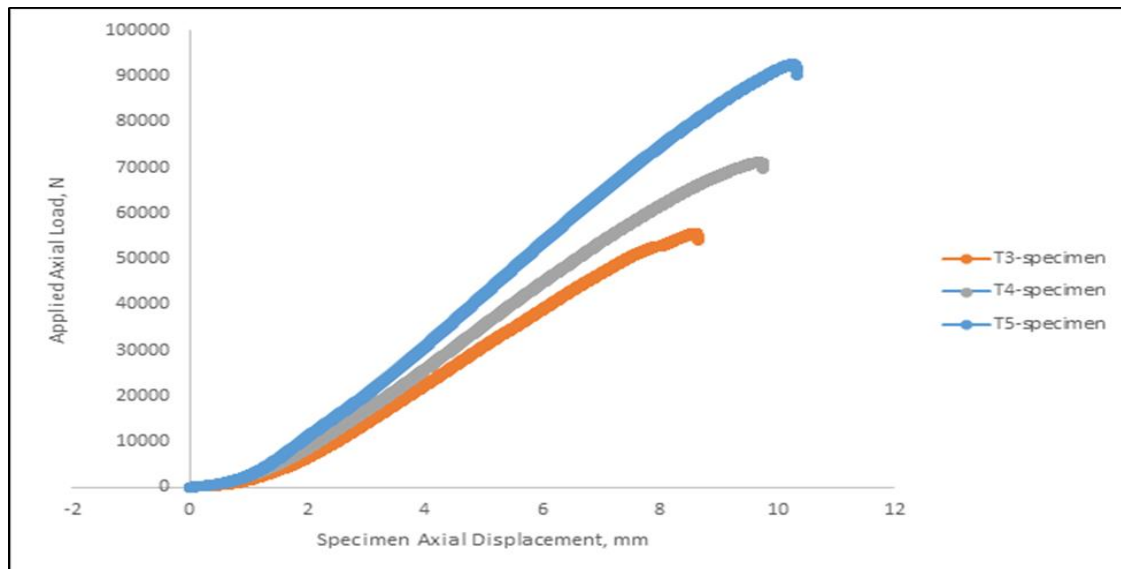
Figure 9: Cross head displacement of test specimens

4.5. Study of Load Distribution Among Two Rows of Bolts

The load distribution in multiple bolted joints is shown in Figure. 10. The load distribution in the two rows of fasteners are computed using methods suggested in literature [30, 31]. The comparison of these percentage load distribution is shown in Figure. 11. It is observed that the in the present case, the loads are not equally distributed between the bolts. This is attributed to the possible difference in the fits between the different bolts and material anisotropy of the specimen laminate.
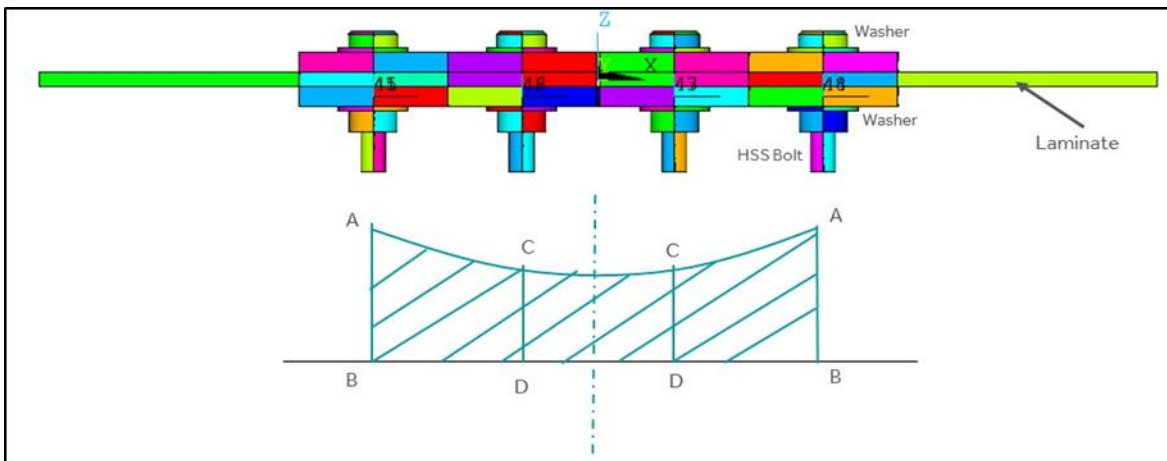
Figure. 10: Fastener load distribution in the multiple bolted butt joint
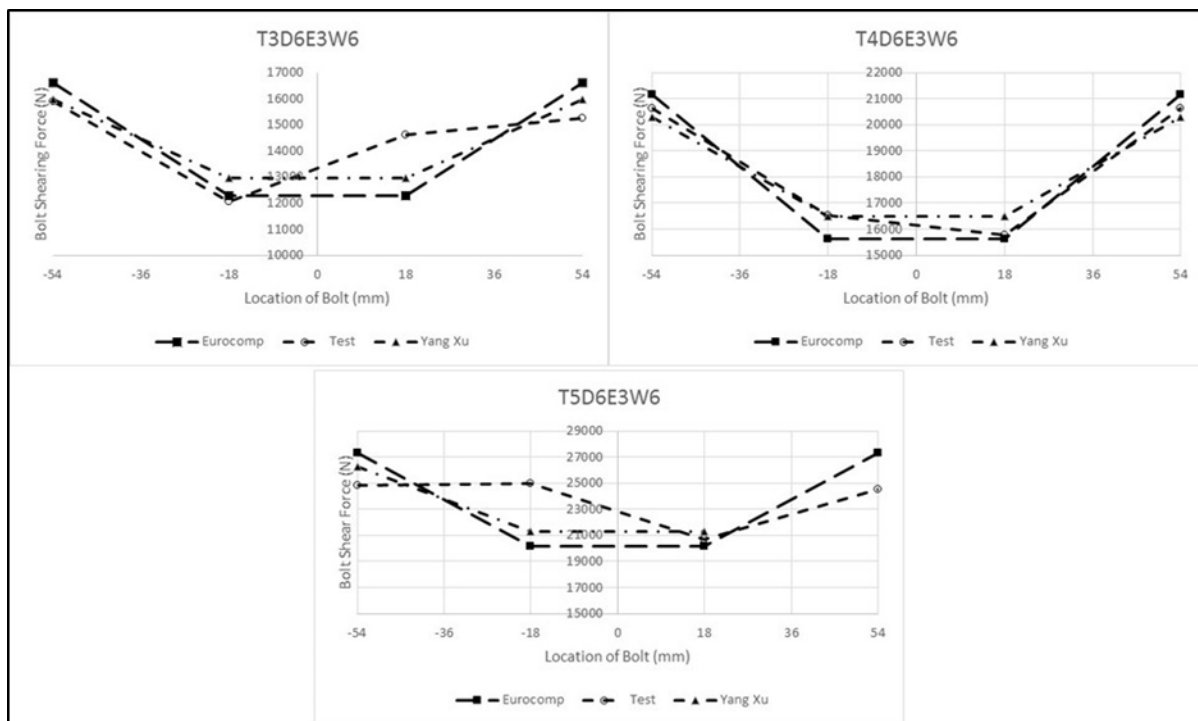
Figure 11: Fastener load distribution in the four bolted butt joint for three types of specimens

4.6. Study of Effect of Specimen Thickness and Material Anisotropy on Bolt Hole Deformation

4.6.1. Bolt Hole Deformation of Specimens of Different Thickness from Test

Figure 12 and 13 show the comparison of axial deformation of the hole from test among specimens of different thickness. It is observed that the deformation of the decreases as the specimen thickness and hence the stiffness increases. It is also observed from Figure 14 that bolt hole deformation at Hole 2 (away from the loading edge) is less when compared to that at Hole 1 (close to the loading edge). Figure 14 shows a comparison of the axial displacement of the bolt hole at the four bolt locations. It can be observed that the displacement of the bolts points is different. Hence, the

stiffness of the specimen is also different at these locations. This observation suggests that the stiffness of the laminate may not be uniform because of the material anisotropy throughout the laminate. Empirical relationships between the Hole 1 deformation (δ) and radius of the undeformed bolt hole (R) are as shown in Table 7.

Table 7: Empirical relations between the bolt hole deformation and radius

Specimen	Empirical Equations for deformation of Hole 1
T3D6E3W6	$\delta_{Hole} = -0.2982R^2Cos^2(\theta) - R*Sin(\theta) + 2.1749$
T4D6E3W6	$\delta_{Hole} = -0.1674R^2Cos^2(\theta) - R*Sin(\theta) + 0.8877$
T5D6E3W6	$\delta_{Hole} = -0.2067R^2Cos^2(\theta) - R*Sin(\theta) + 1.4204$
Specimen	**Empirical Equations for deformation of Hole 2**
T3D6E3W6	$\delta_{Hole} = -0.2173R^2Cos^2(\theta) - R*Sin(\theta) + 1.6295$
T4D6E3W6	$\delta_{Hole} = -0.2084R^2Cos^2(\theta) + 1.1513$
T5D6E3W6	$\delta_{Hole} = -0.2318R^2Cos^2(\theta) - R*Sin(\theta) + 1.7651$
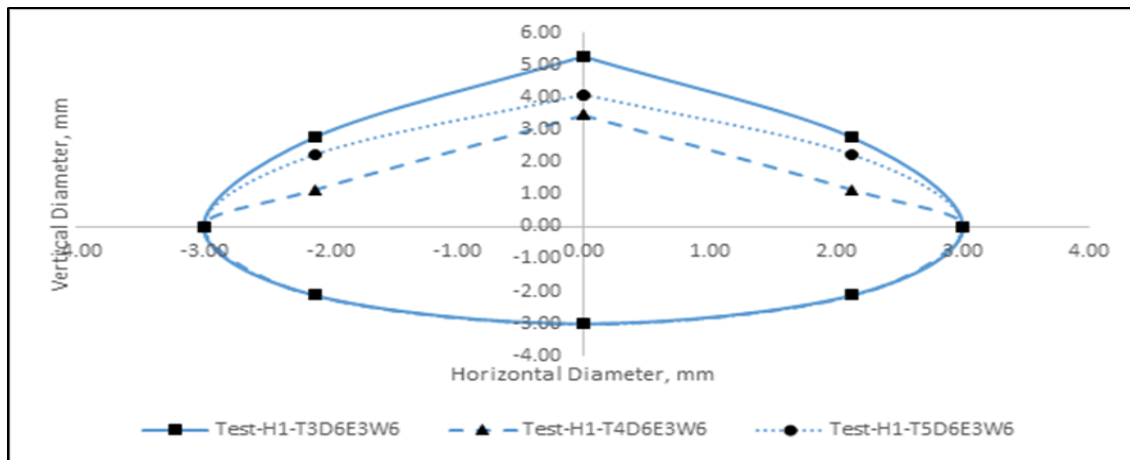
Figure 12: Deformation of bolt hole for three specimens from test - Hole 1
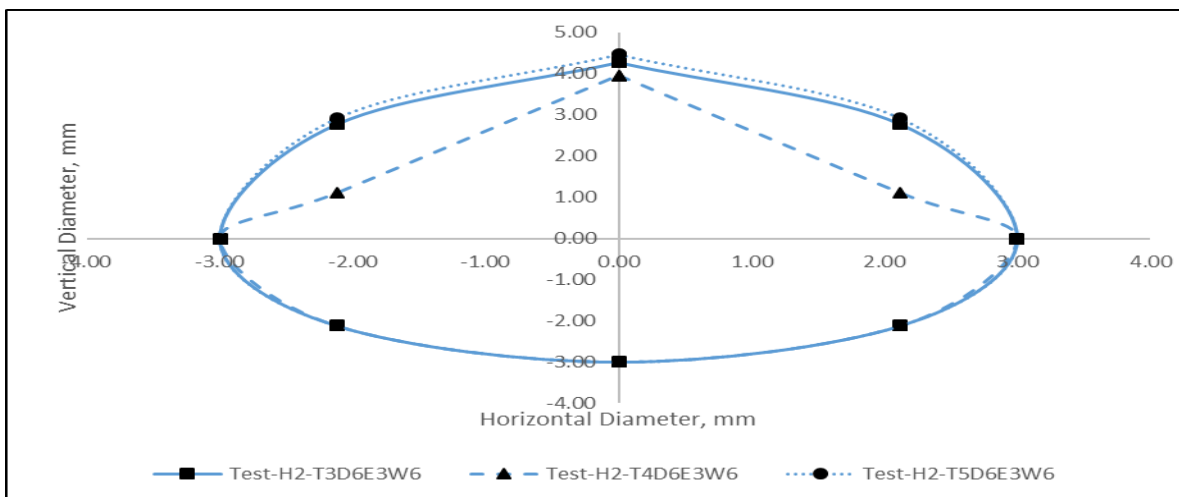
Figure 13: Deformation of bolt hole for three specimens from test - Hole 2
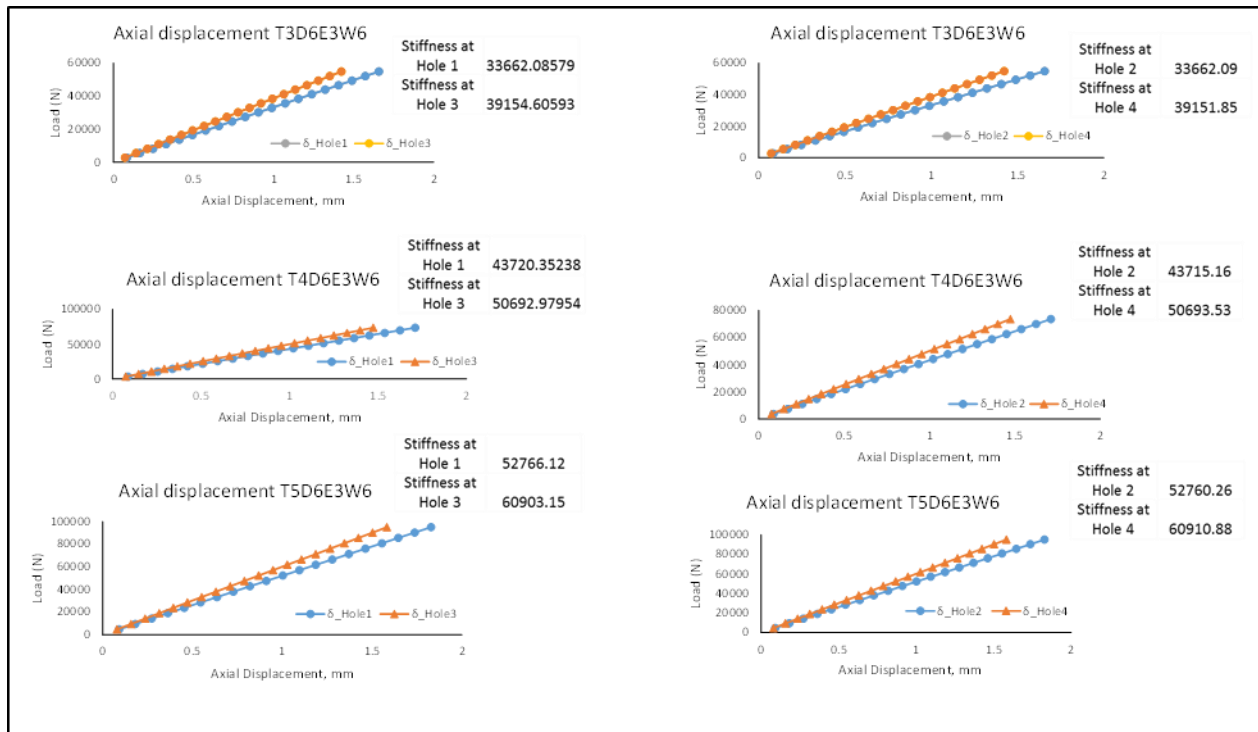
Figure 14: Axial deformation of bolt holes for three specimens form FEA

4.6.2. *Effect of Fit on Hole Deformation of Specimens of Different Thickness*

Figure 15 and 16 show the finite element simulation results with effect of friction coefficient ($\mu = 0$ and $\mu = 0.1$) on the bolt hole deformation for three specimens. It is observed that the deformation of the holes of three different thickness specimens is affected to a negligible extent with the introduction of a friction coefficient.
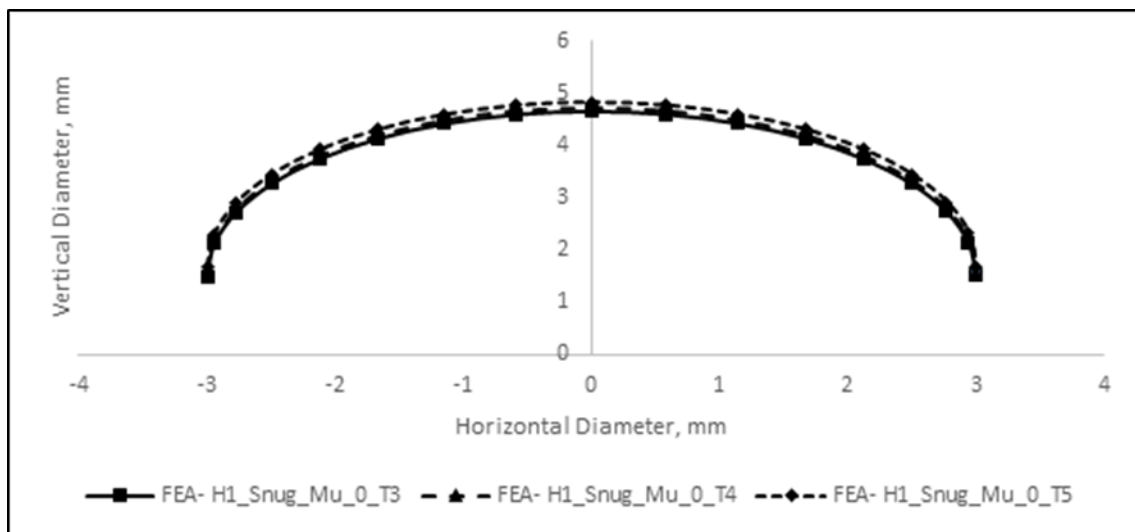
Figure 15: Deformation of bolt hole for three types of specimens - Hole 1($\mu = 0$)
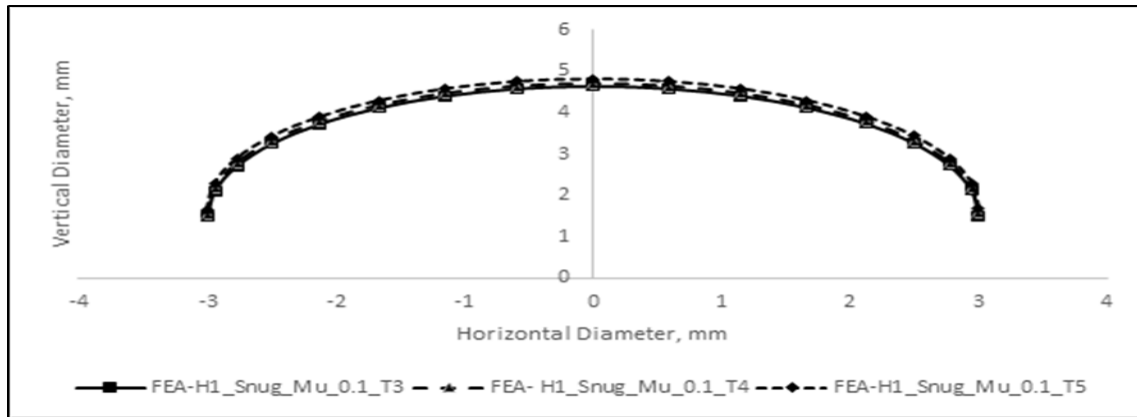
Figure 16: Deformation of bolt hole for three types of specimens - Hole 1 (μ = 0.1)

4.6.3. *Comparison of Bolt Hole Deformation Between FEA and Test for Different Values of Friction - Snug Fit*

Figure 17 and 18 show the comparison of the bolt hole deformation for between the test and finite element analysis with two different values of friction (0 and 0.1). It is observed that the deformation of the holes in test is slightly more as compared to the prediction by finite element analysis for both values of friction. Also, it is observed that the increase in the coefficient of friction doesn't affect the deformation of the hole.
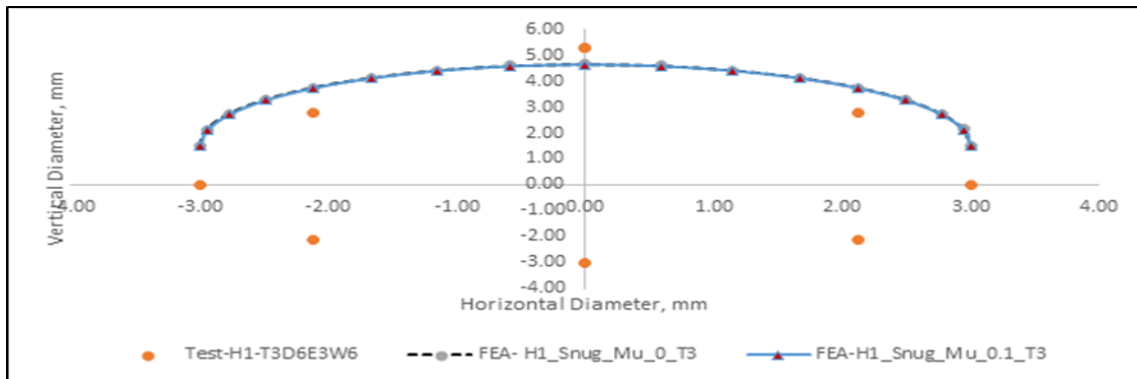

Figure 17: Comparison of deformation of bolt hole for Test and Snug fit - Hole 1 (μ = 0 and 0.1)
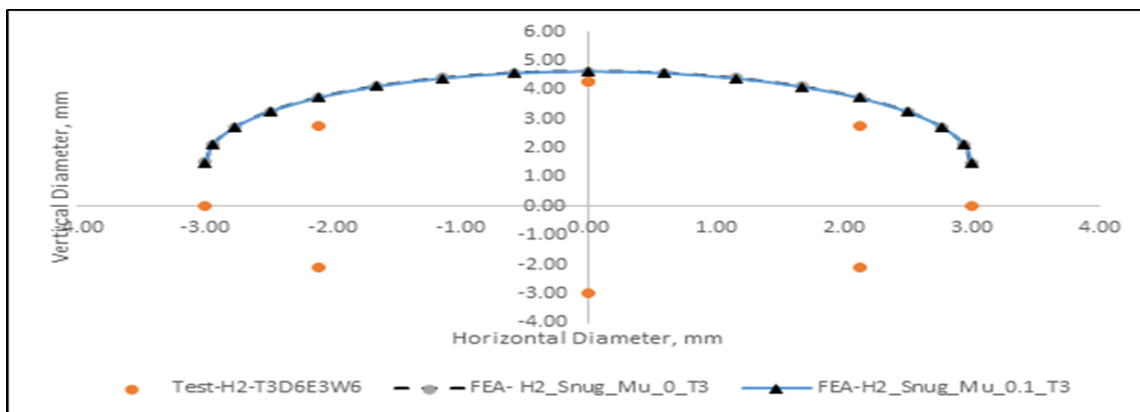
Figure 18: Comparison of deformation of bolt hole for Test and Snug fit - Hole 2 (μ = 0 and 0.1)

4.6.4. Comparison of Bolt Hole Deformation Between FEA And Test for Different Values of Friction - Interference Fit

Figure 19 and 20 show the comparison of the bolt hole deformation for between the test and finite element analysis with two different values of friction (0 and 0.1). It is observed that the deformation of the holes in test is slightly more as compared to the prediction by finite element analysis for both values of friction. Also, it is observed that the increase in the coefficient of friction doesn't affect the deformation of the hole.
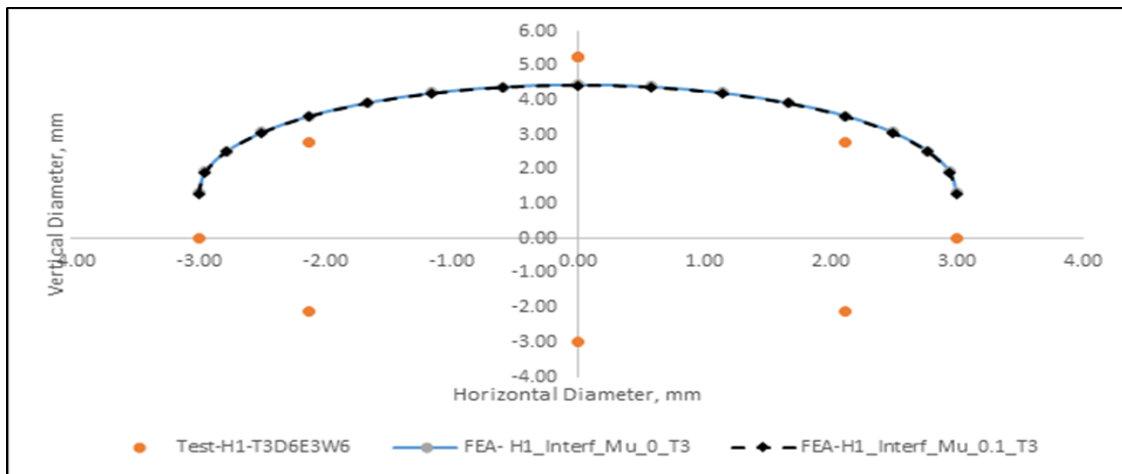
Figure 19: Comparison of deformation of bolt hole for Test and Interference fit - Hole 1 (μ = 0 and 0.1, Interference = 0.16 mm)
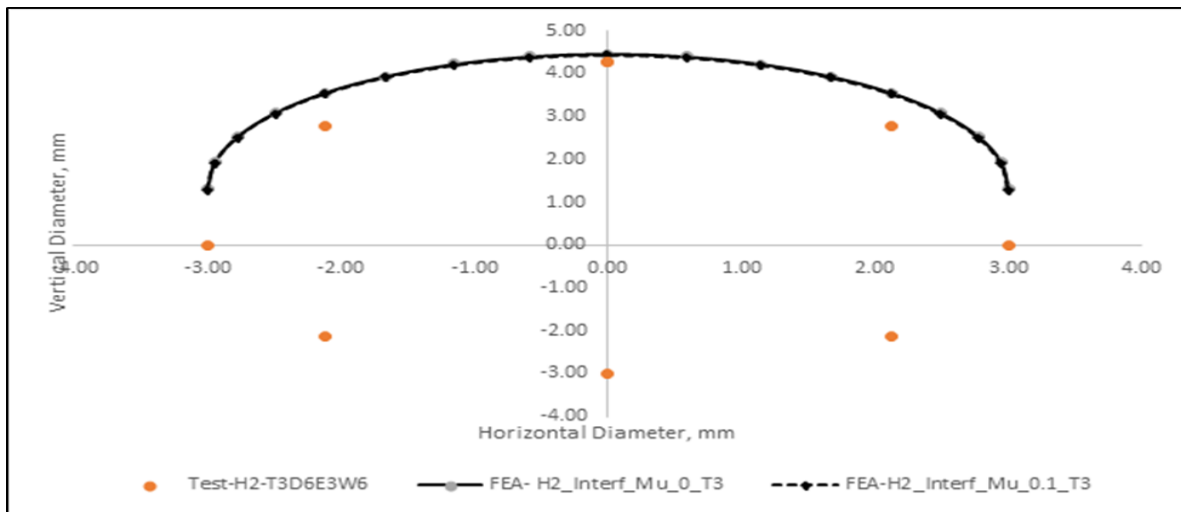
Figure 20: Comparison of deformation of bolt hole for Test and Interference fit - Hole 2 (μ = 0 and 0.1, Interference of 0.16 mm)

4.6.5. Comparison of Bolt Hole Deformation Between FEA and Test for Different Values of Friction - Clearance Fit

Figure 21 and 22 show the comparison of the bolt hole deformation for between the test and finite element analysis with two different values of friction (0 and 0.1). It is observed that the

deformation of the holes in test is slightly more as compared to the prediction by finite element analysis for both values of friction. Also, it is observed that the increase in the coefficient of friction doesn't affect the deformation of the hole.
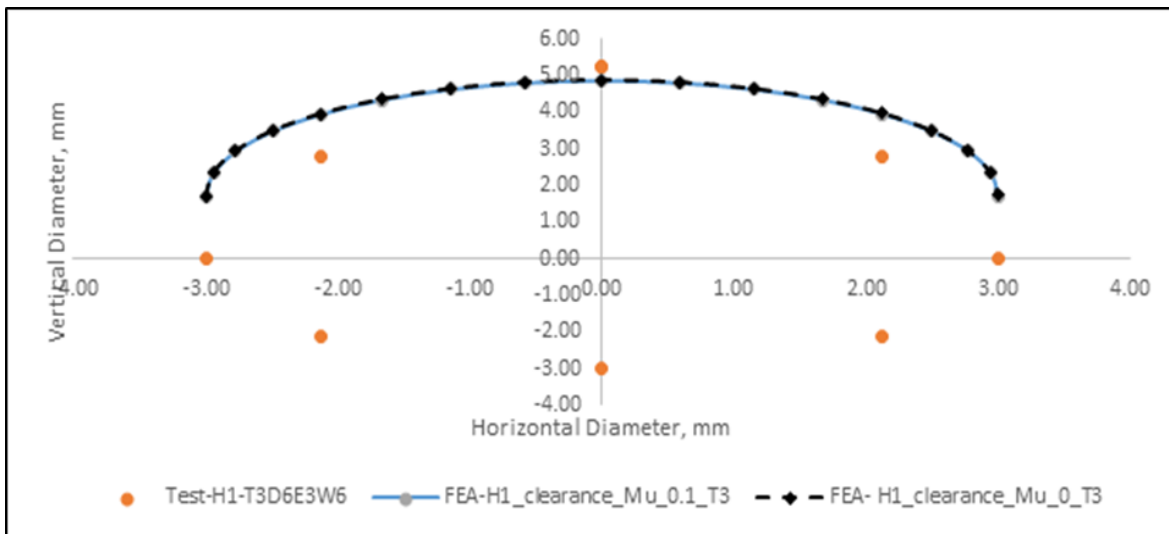
Figure 21: Comparison of deformation of bolt hole for Test and Clearance fit - Hole 1 (μ = 0 and 0.1 Clearance of 0.079 mm)
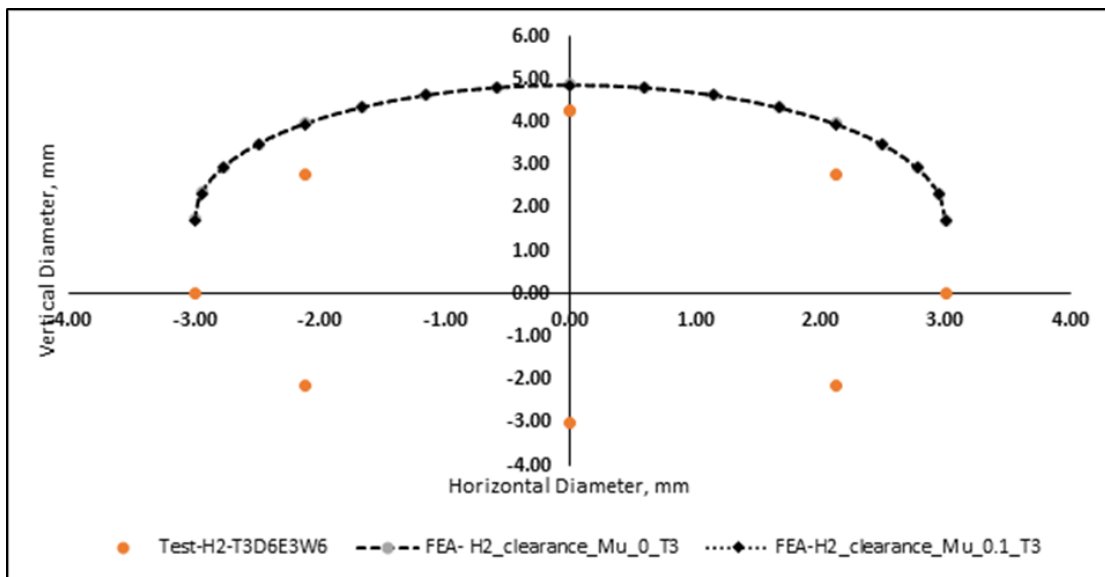
Figure 22: Comparison of deformation of bolt hole for Test and Clearance fit - Hole 2 (μ = 0 and 0.1 and Clearance of 0.079 mm)

4.7. Study of Effect of Anisotropy and Type of Bolt Fit on Contact Stresses at Bolt Holes

Effect of anisotropy / type of bolt fit on the contact stresses is studied in the butt joint by considering a quasi-isotropic laminate specimens of three different thicknesses (Figure. 23 to 46). In this butt joint configuration, the effect of normal and shear loading on contact stresses and the contact region is captured. The variation of contact stresses along the boundary of the hole for the

case of a snug fit, interference fit and clearance fit are presented. It is observed that while the circumferential and shear stresses show small variation in the magnitude, the radial stress doesn't show much difference. The distribution of the stress varies along the circumference with the change in type of fit. The set of stresses at any point (r,θ) are given by the following expressions [33]

$$\sigma_r = \frac{\sigma_\infty}{2}\left[1 - \frac{a^2}{r^2} + G\left(1 - 4\frac{a^2}{r^2} + 3\frac{a^4}{r^4}\right)Cos\,2\theta\right] \qquad (11)$$

$$\sigma_\theta = \frac{\sigma_\infty}{2}\left[1 + \frac{a^2}{r^2} - G\left(1 + 3\frac{a^4}{r^4}\right)Cos\,2\theta\right] \qquad (12)$$

$$\tau_{r\theta} = -\frac{\sigma_\infty}{2}G\left[1 + \frac{a^2}{r^2} - 3\frac{a^4}{r^4}Sin\,2\theta\right] \qquad (13)$$

$$\text{Where,}\quad G = \frac{E_s}{(E_s)_\infty} \qquad (14)$$

For the state of elastic stress, Secant Modulus Es is replaced by the Young's modulus and thus G = 1.0
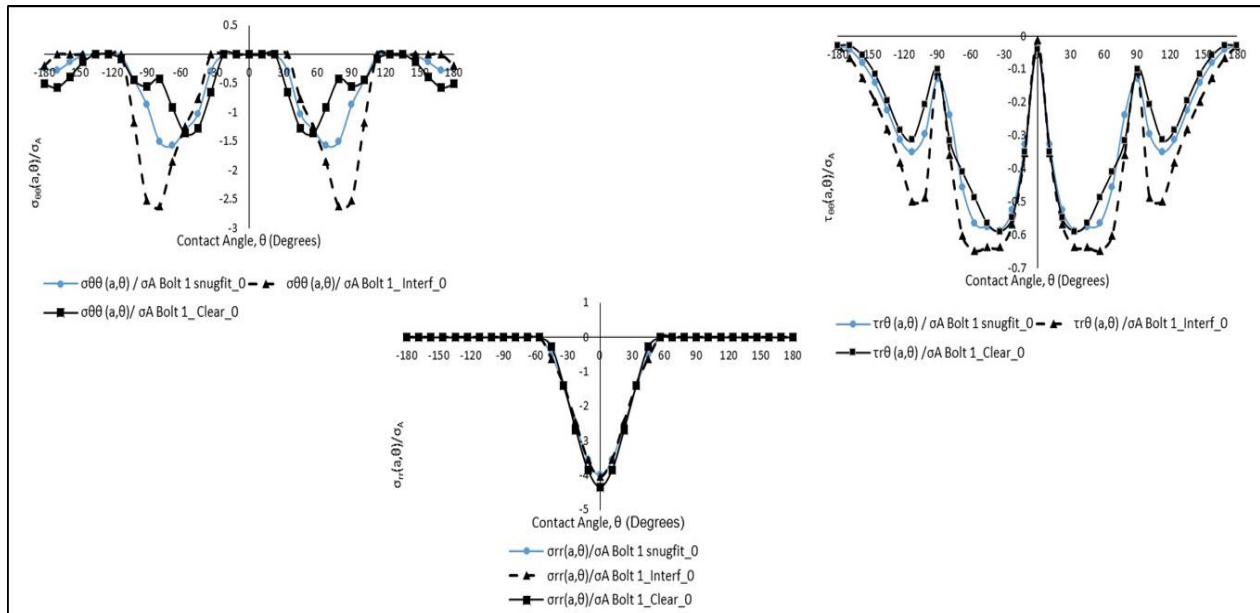

Figure 23: The effect of snug, interference and clearance fits on tangential, radial and shear contact stresses in a double lap butt joint of GFRP laminates with AA 6061-T4 butt straps for a quasi-isotropic layup in the presence of bearing and bypass loading along the boundary of the pin-loaded hole (Bolt 1: Torque = 2.2 N-m, μ= 0.0, Thickness = 3.326 mm)
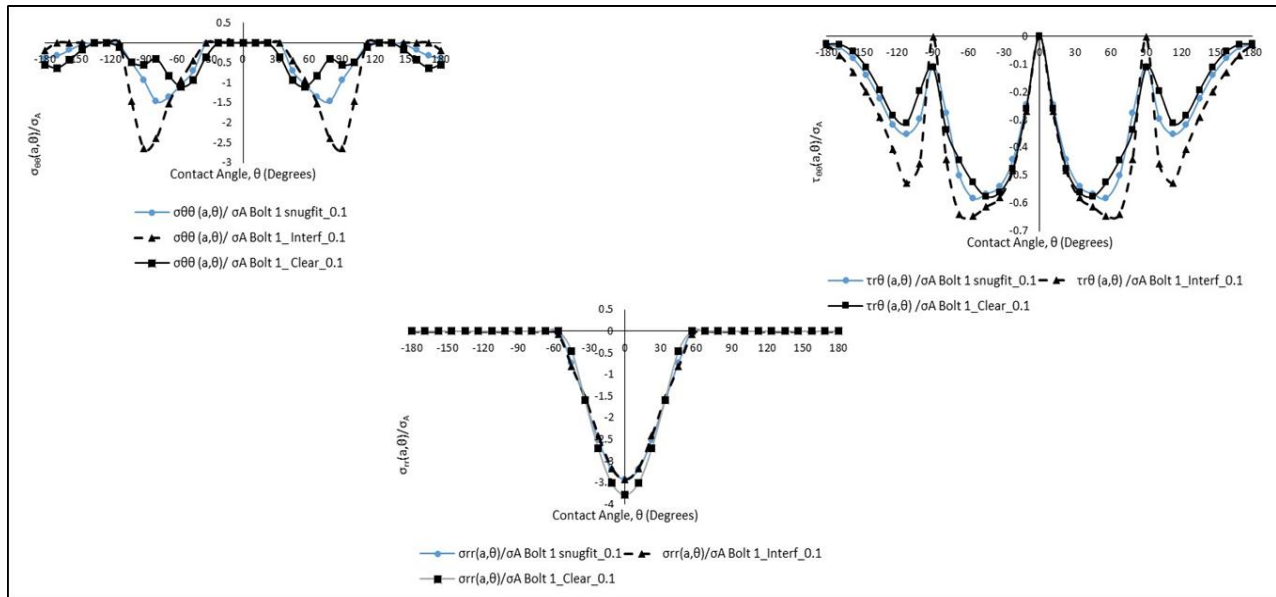
Figure 24: The effect of snug, interference and clearance fits on tangential, radial and shear contact stresses in a double lap butt joint of GFRP laminates with AA 6061-T4 butt straps for a quasi-isotropic layup in the presence of bearing and bypass loading along the boundary of the pin-loaded hole (Bolt 1: Torque = 2.2 N-m, μ= 0.1, Thickness = 3.326 mm)
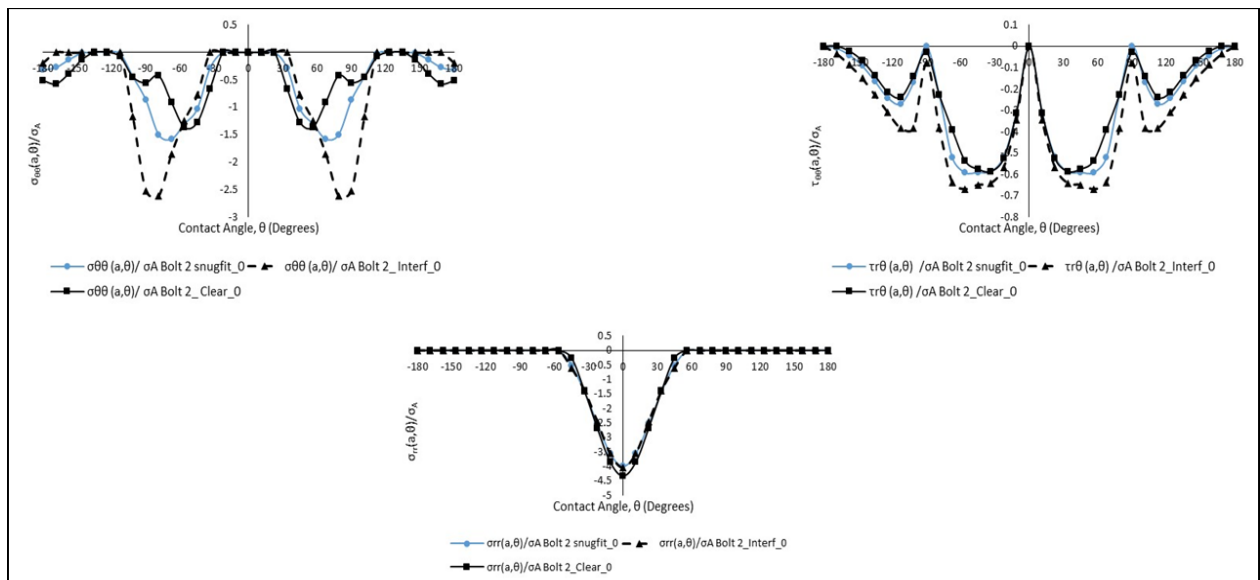
Figure 25: The effect of snug, interference and clearance fits on tangential, radial and shear contact stresses in a double lap butt joint of GFRP laminates with AA 6061-T4 butt straps for a quasi-isotropic layup in the presence of bearing and bypass loading along the boundary of the pin-loaded hole (Bolt 2: Torque = 2.2 N-m, μ= 0.0, Thickness = 3.326 mm)
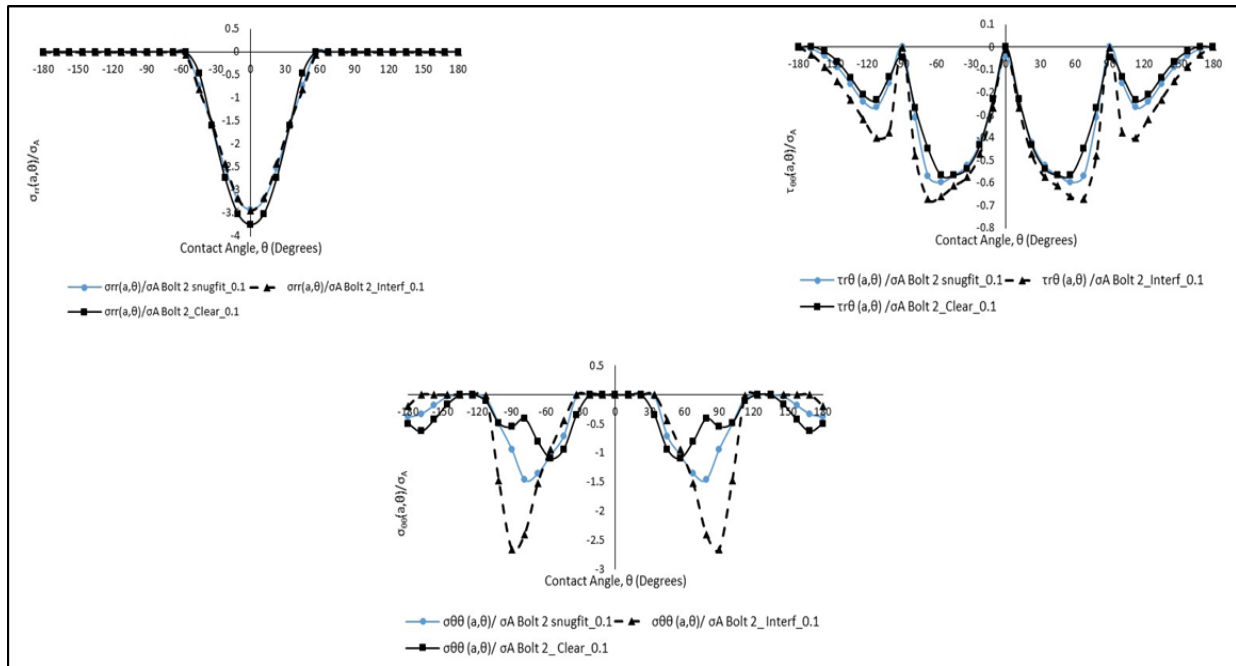
Figure 26: The effect of snug, interference and clearance fits on tangential, radial and shear contact stresses in a double lap butt joint of GFRP laminates with AA 6061-T4 butt straps for a quasi-isotropic layup in the presence of bearing and bypass loading along the boundary of the pin-loaded hole (Bolt 2: Torque = 2.2 N-m, μ= 0.1, Thickness = 3.326 mm)
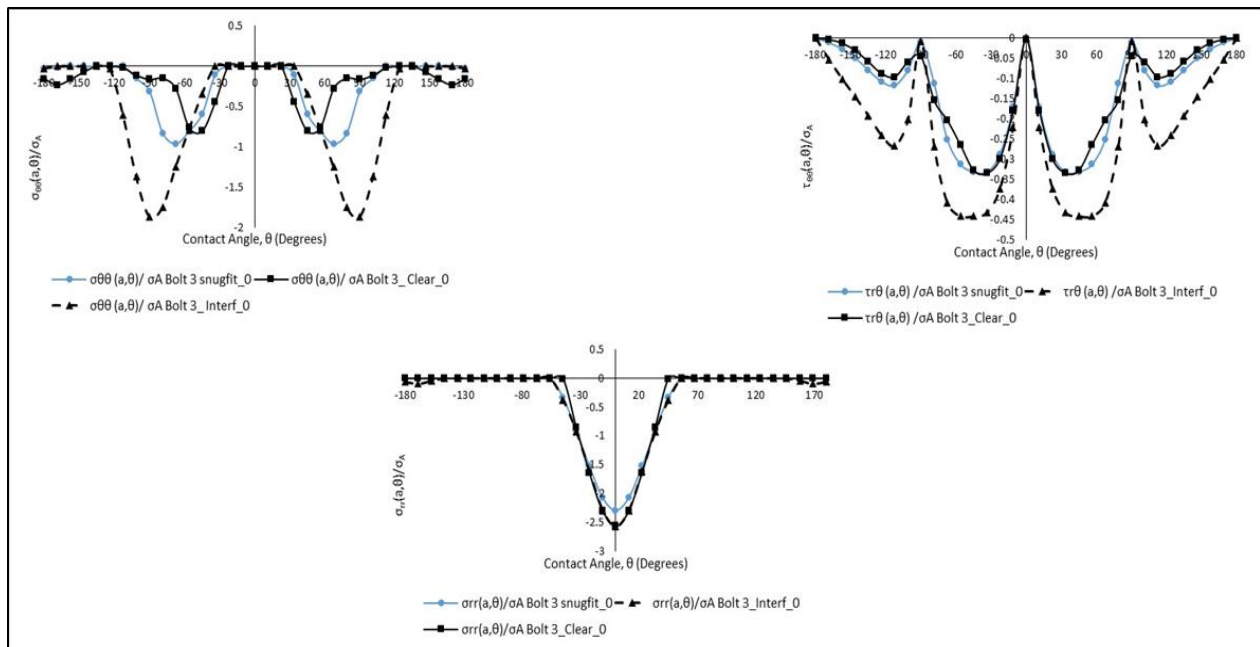

Figure 27: The effect of snug, interference and clearance fits on tangential, radial and shear contact stresses in a double lap butt joint of GFRP laminates with AA 6061-T4 butt straps for a quasi-isotropic layup in the presence of bearing and bypass loading along the boundary of the pin-loaded hole (Bolt 3: Torque = 2.2 N-m, μ= 0.0, Thickness = 3.326 mm)
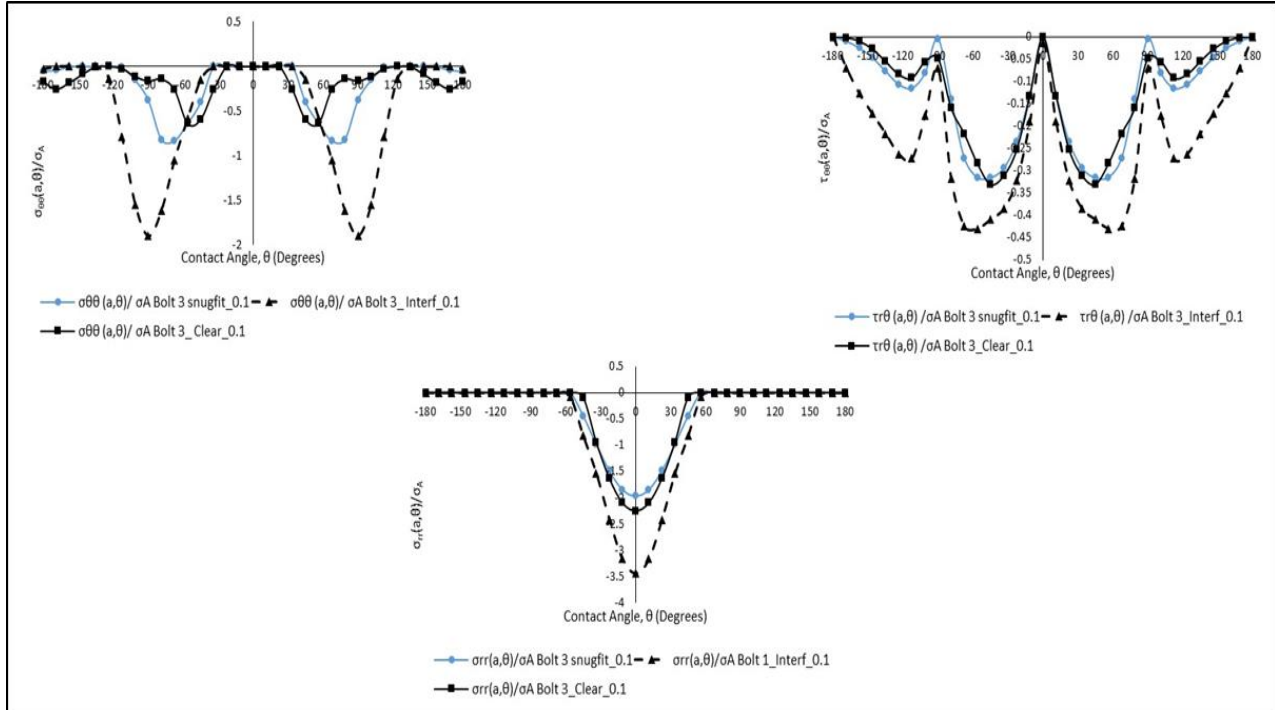
Figure 28: The effect of snug, interference and clearance fits on tangential, radial and shear contact stresses in a double lap butt joint of GFRP laminates with AA 6061-T4 butt straps for a quasi-isotropic layup in the presence of bearing and bypass loading along the boundary of the pin-loaded hole (Bolt 3: Torque = 2.2 N-m, μ= 0.1, Thickness = 3.326 mm)
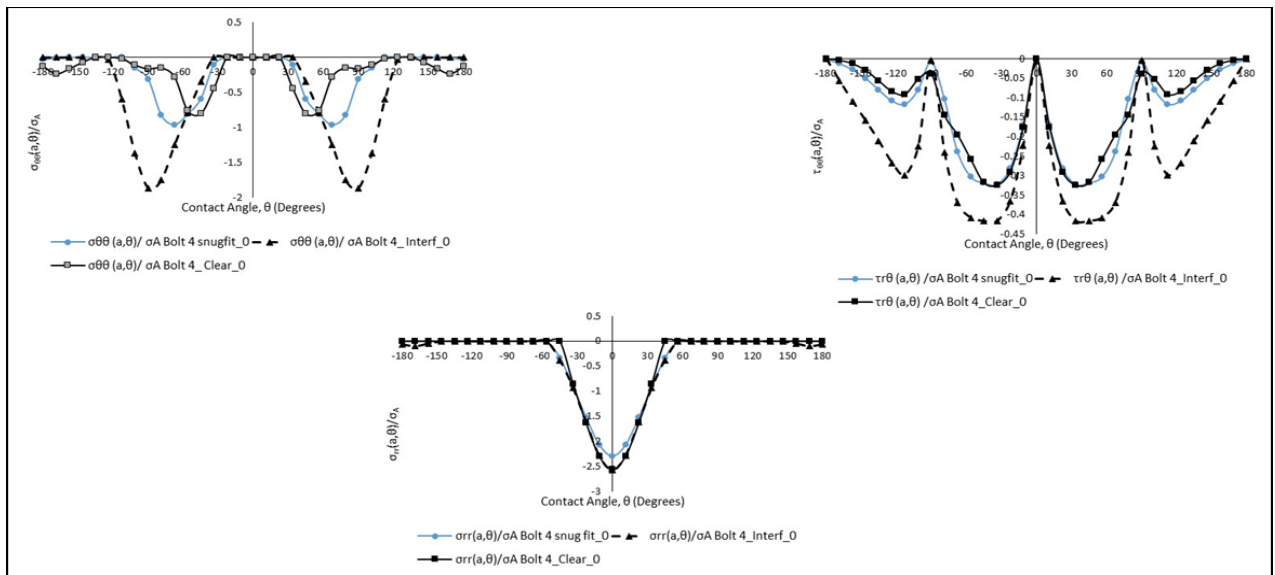

Figure 29: The effect of snug, interference and clearance fits on tangential, radial and shear contact stresses in a double lap butt joint of GFRP laminates with AA 6061-T4 butt straps for a quasi-isotropic layup in the presence of bearing and bypass loading along the boundary of the pin-loaded hole (Bolt 4: Torque = 2.2 N-m, μ= 0.0, Thickness = 3.326 mm)
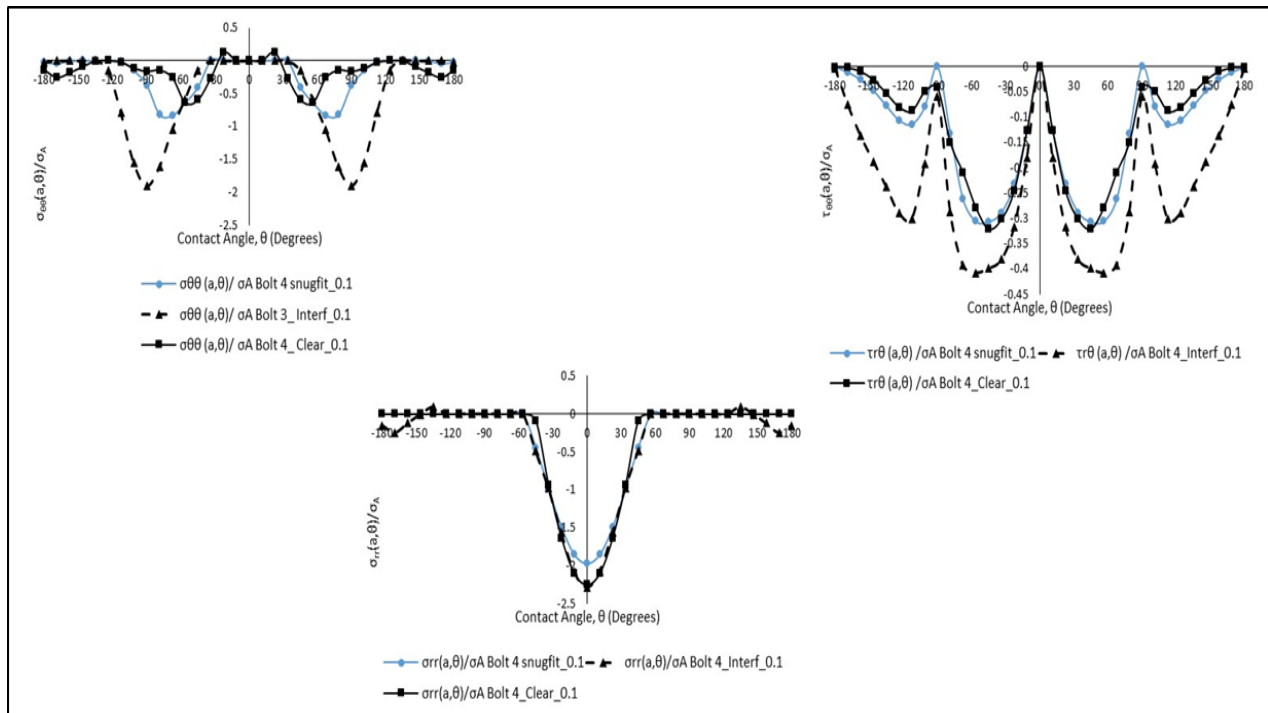
Figure 30: The effect of snug, interference and clearance fits on tangential, radial and shear contact stresses in a double lap butt joint of GFRP laminates with AA 6061-T4 butt straps for a quasi-isotropic layup in the presence of bearing and bypass loading along the boundary of the pin-loaded hole (Bolt 4: Torque = 2.2 N-m, μ= 0.1, Thickness = 3.326 mm)
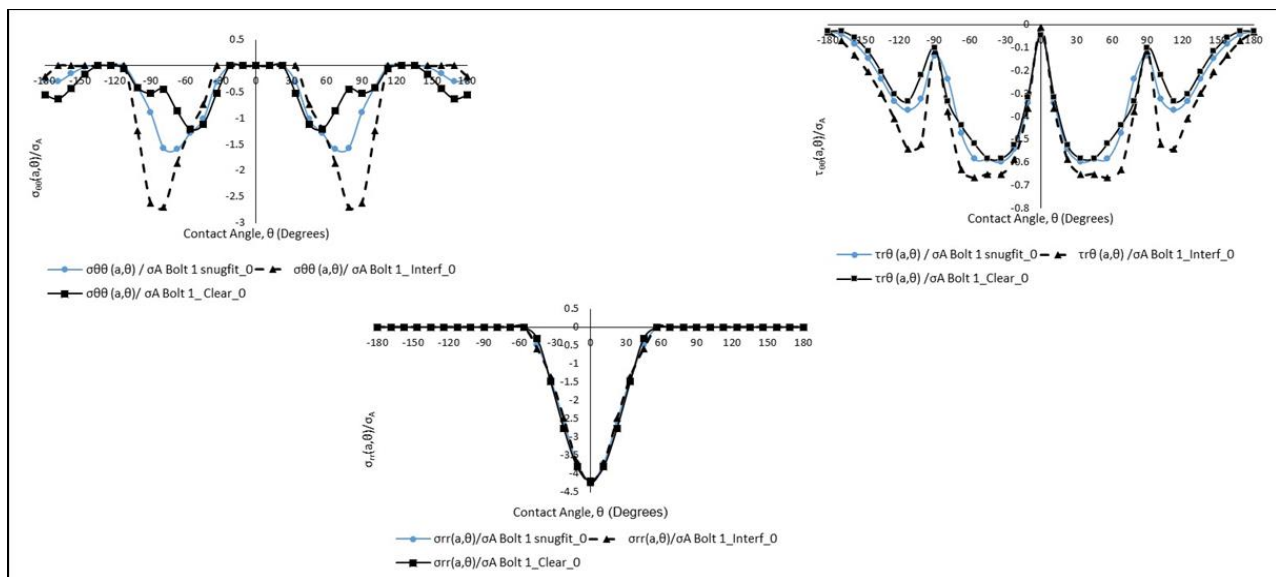
Figure 31: The effect of snug, interference and clearance fits on tangential, radial and shear contact stresses in a double lap butt joint of GFRP laminates with AA 6061-T4 butt straps for a quasi-isotropic layup in the presence of bearing and bypass loading along the boundary of the pin-loaded hole (Bolt 1: Torque = 2.2 N-m, μ= 0.0, Thickness = 4.5 mm)
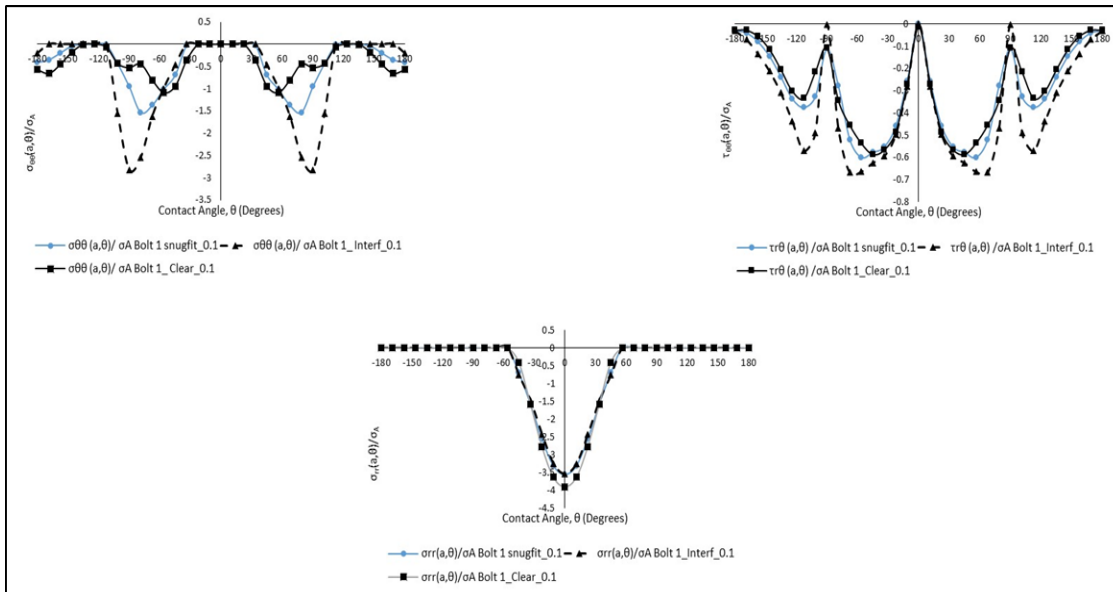
Figure 32: Effect of snug, interference and clearance fits on tangential, radial and shear contact stresses in a double lap butt joint of GFRP laminates with AA 6061-T4 butt straps for a quasi-isotropic layup in the presence of bearing and bypass loading along the boundary of the pin-loaded hole (Bolt 1: Torque = 2.2 N-m, μ= 0.1, Thickness = 4.5 mm)
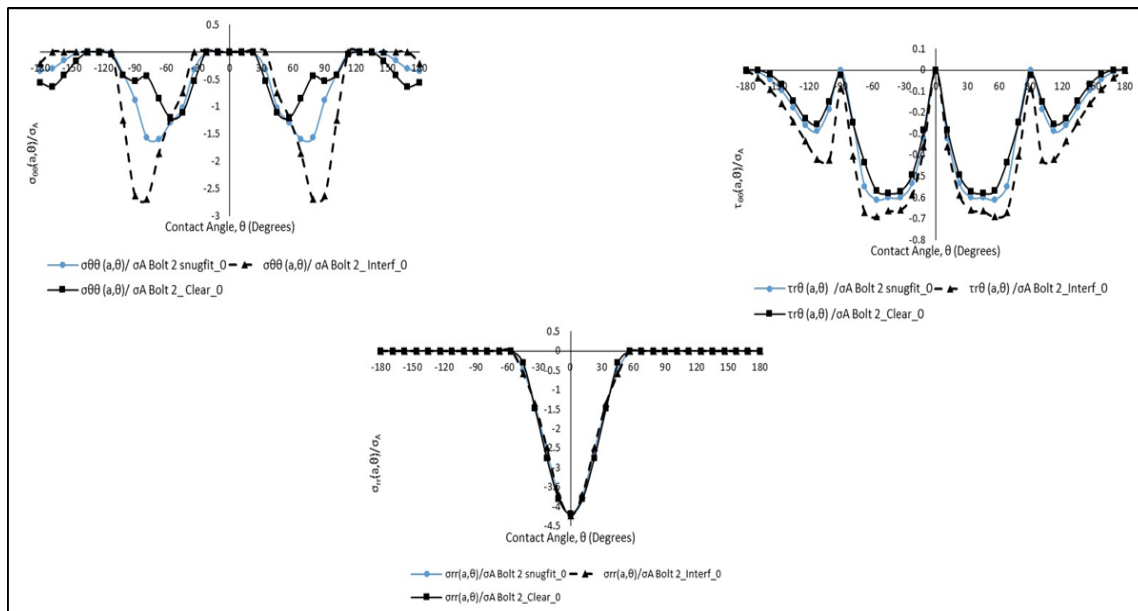

Figure 33: Effect of snug, interference and clearance fits on tangential, radial and shear contact stresses in a double lap butt joint of GFRP laminates with AA 6061-T4 butt straps for a quasi-isotropic layup in the presence of bearing and bypass loading along the boundary of the pin-loaded hole (Bolt 2: Torque = 2.2 N-m, μ= 0.0, Thickness = 4.5 mm)
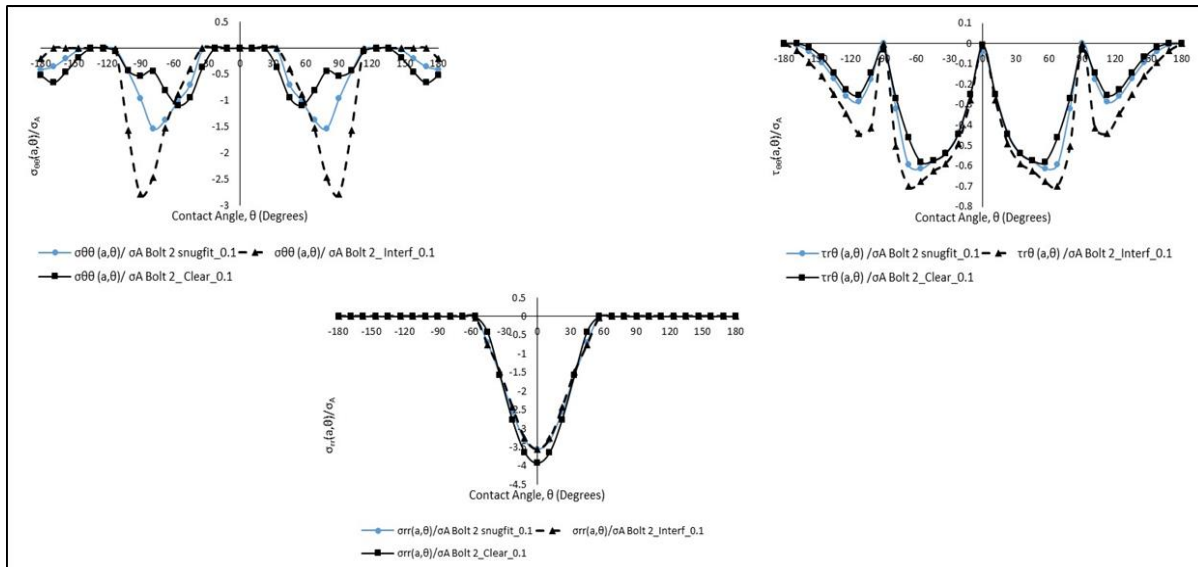
Figure 34: Effect of snug, interference and clearance fits on tangential, radial and shear contact stresses in a double lap butt joint of GFRP laminates with AA 6061-T4 butt straps for a quasi-isotropic layup in the presence of bearing and bypass loading along the boundary of the pin-loaded hole (Bolt 2: Torque = 2.2 N-m, μ= 0.1, Thickness = 4.5 mm)
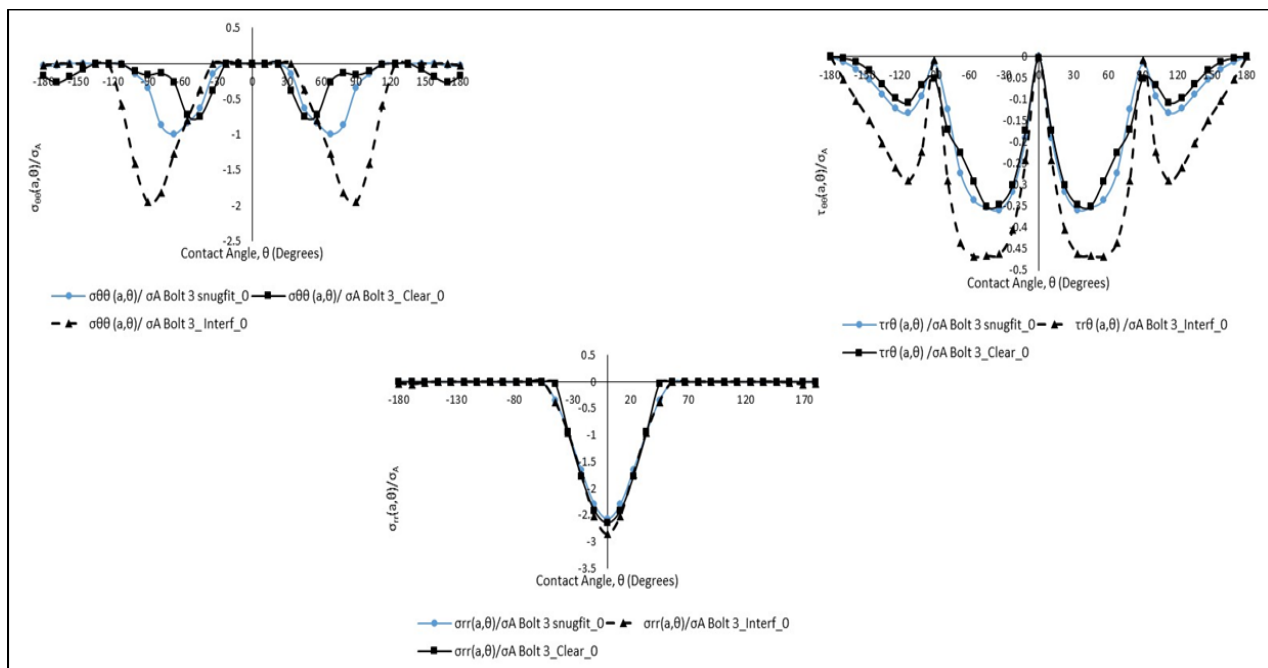

Figure 35 Effect of snug, interference and clearance fits on tangential, radial and shear contact stresses in a double lap butt joint of GFRP laminates with AA 6061-T4 butt straps for a quasi-isotropic layup in the presence of bearing and bypass loading along the boundary of the pin-loaded hole (Bolt 3: Torque = 2.2 N-m, μ= 0.0, Thickness = 4.5 mm)
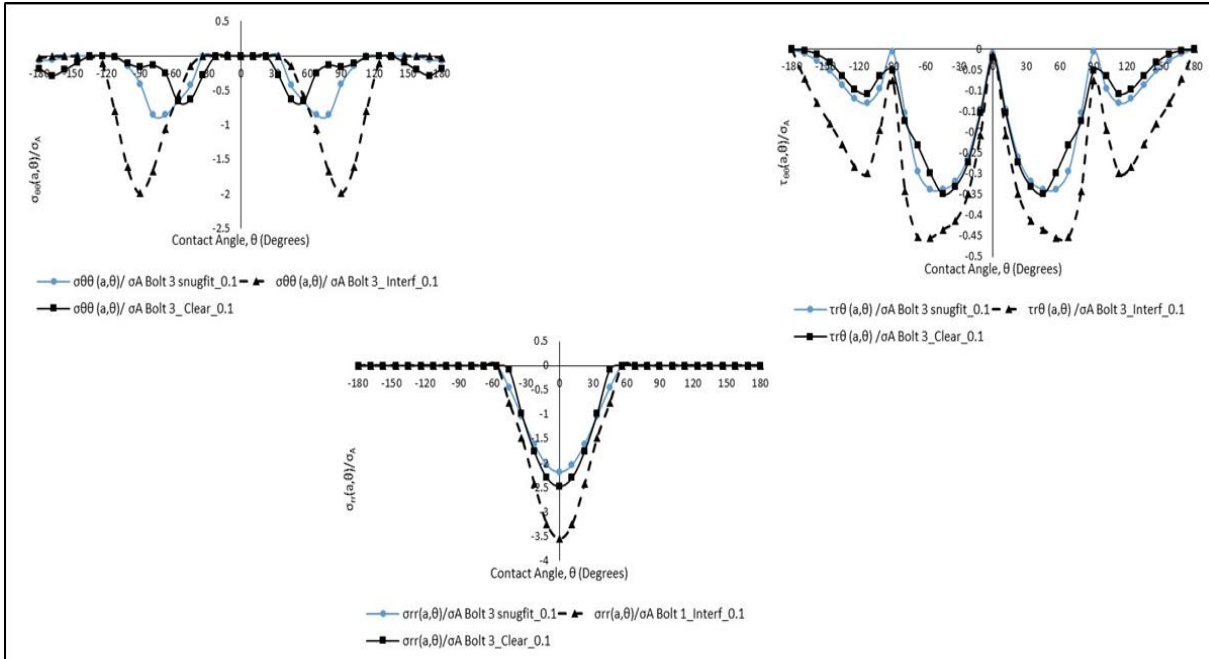
Figure 36: Effect of snug, interference and clearance fits on tangential, radial and shear contact stresses in a double lap butt joint of GFRP laminates with AA 6061-T4 butt straps for a quasi-isotropic layup in the presence of bearing and bypass loading along the boundary of the pin-loaded hole (Bolt 3: Torque = 2.2 N-m, μ= 0.1, Thickness = 4.5 mm)
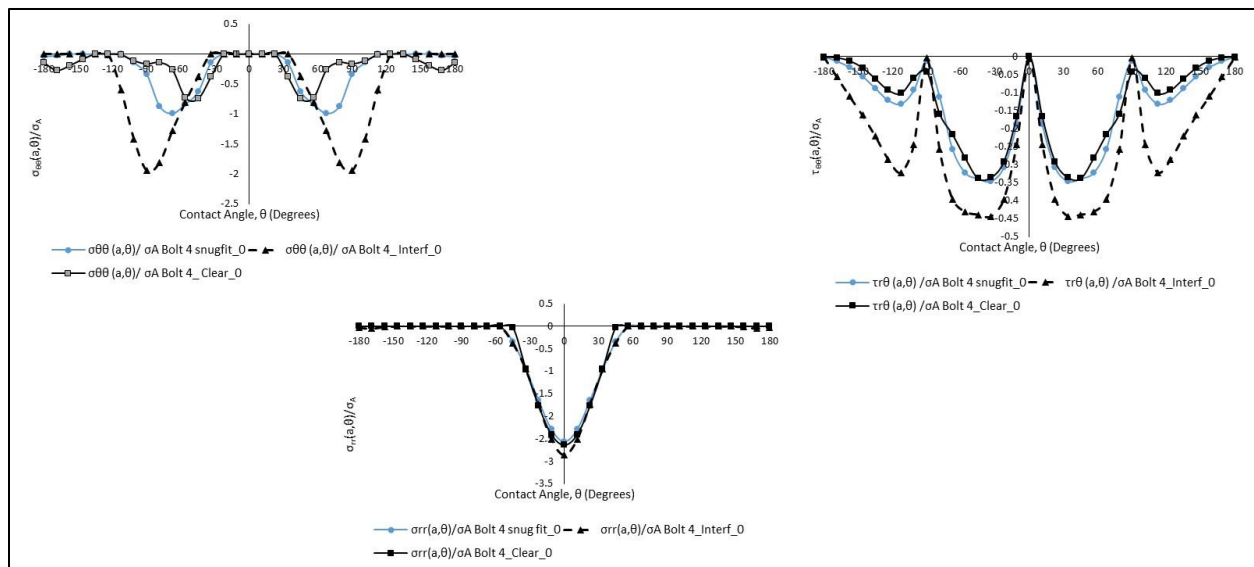

Figure 37 Effect of snug, interference and clearance fits on tangential, radial and shear contact stresses in a double lap butt joint of GFRP laminates with AA 6061-T4 butt straps for a quasi-isotropic layup in the presence of bearing and bypass loading along the boundary of the pin-loaded hole (Bolt 4: Torque = 2.2 N-m, μ= 0.0, Thickness = 4.5 mm)
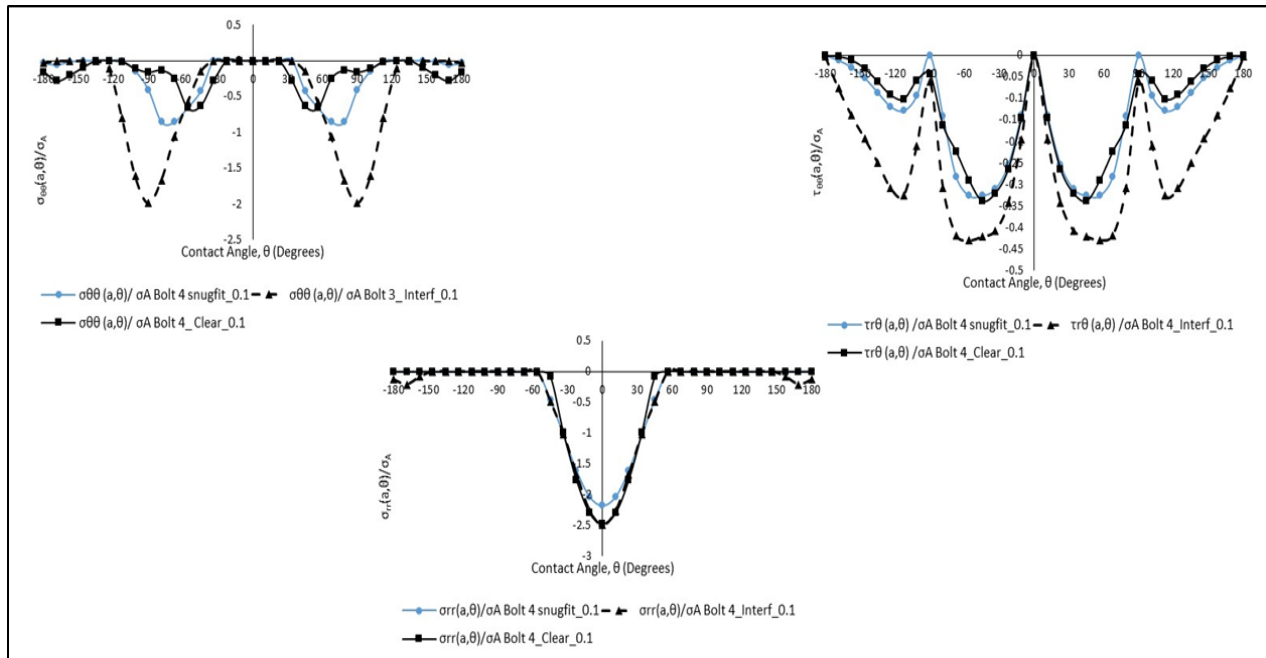
Figure 38: Effect of snug, interference and clearance fits on tangential, radial and shear contact stresses in a double lap butt joint of GFRP laminates with AA 6061-T4 butt straps for a quasi-isotropic layup in the presence of bearing and bypass loading along the boundary of the pin-loaded hole (Bolt 4: Torque = 2.2 N-m, μ= 0.1, Thickness = 4.5 mm)
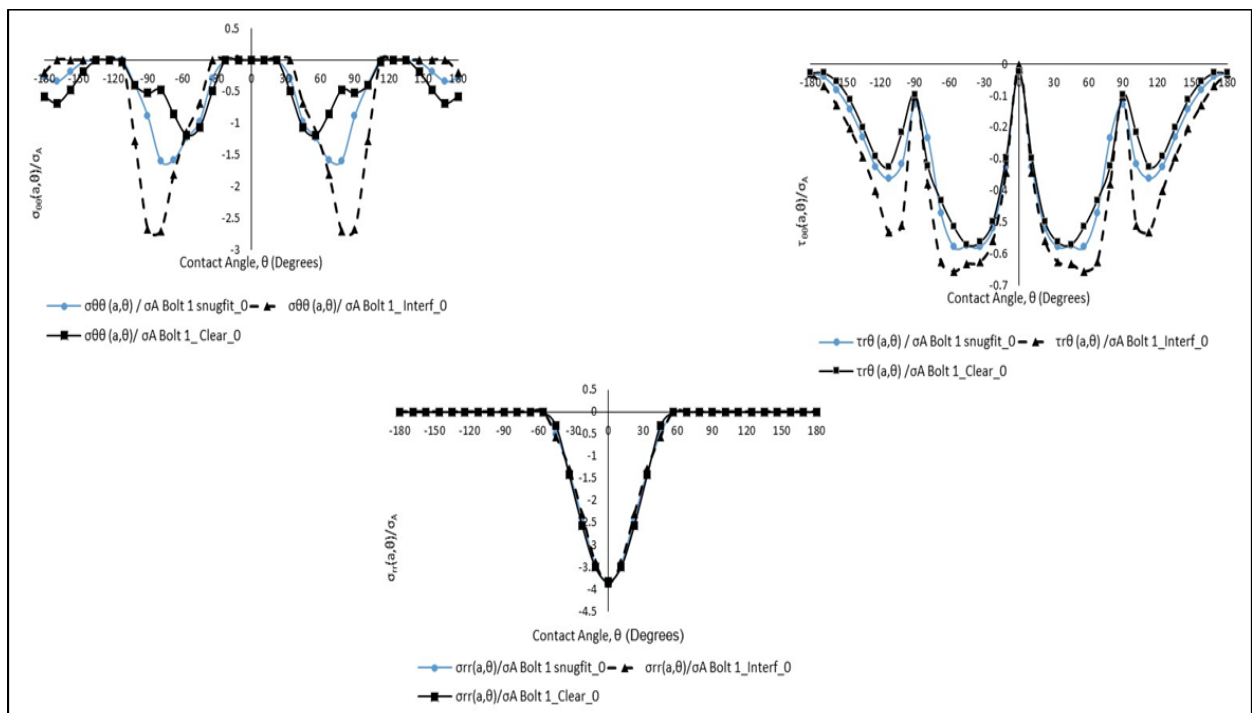

Figure 39: Effect of snug, interference and clearance fits on tangential, radial and shear contact stresses in a double lap butt joint of GFRP laminates with AA 6061-T4 butt straps for a quasi-isotropic layup in the presence of bearing and bypass loading along the boundary of the pin-loaded hole (Bolt 1: Torque = 2.2 N-m, μ= 0.0, Thickness = 5.672 mm)
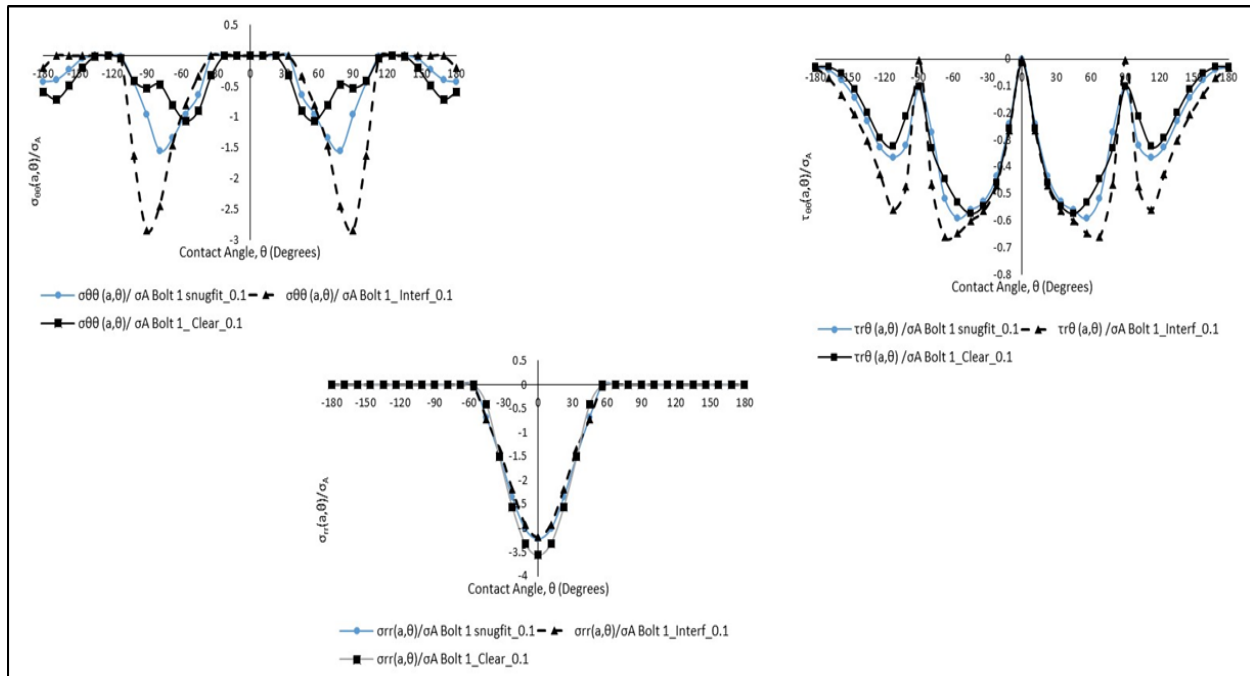
Figure 40: Effect of snug, interference and clearance fits on tangential, radial and shear contact stresses in a double lap butt joint of GFRP laminates with AA 6061-T4 butt straps for a quasi-isotropic layup in the presence of bearing and bypass loading along the boundary of the pin-loaded hole (Bolt 1: Torque = 2.2 N-m, μ= 0.1, Thickness = 5.672 mm)
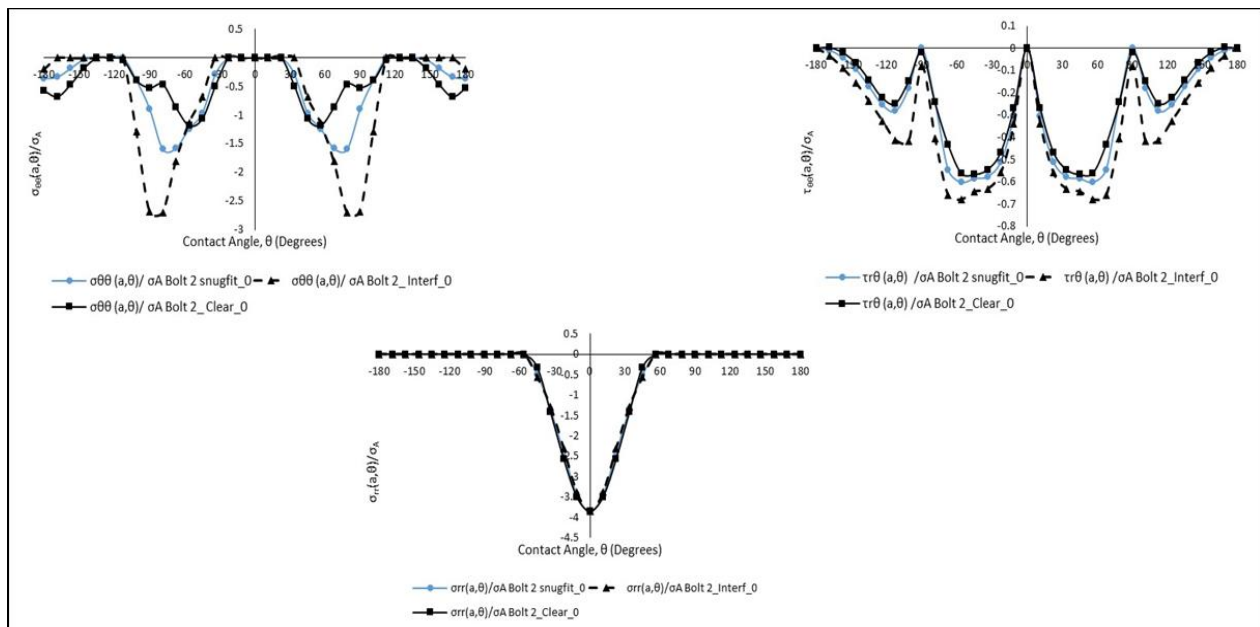
Figure 41: Effect of snug, interference and clearance fits on tangential, radial and shear contact stresses in a double lap butt joint of GFRP laminates with AA 6061-T4 butt straps for a quasi-isotropic layup in the presence of bearing and bypass loading along the boundary of the pin-loaded hole (Bolt 2: Torque = 2.2 N-m, μ= 0.0, Thickness = 5.672 mm)
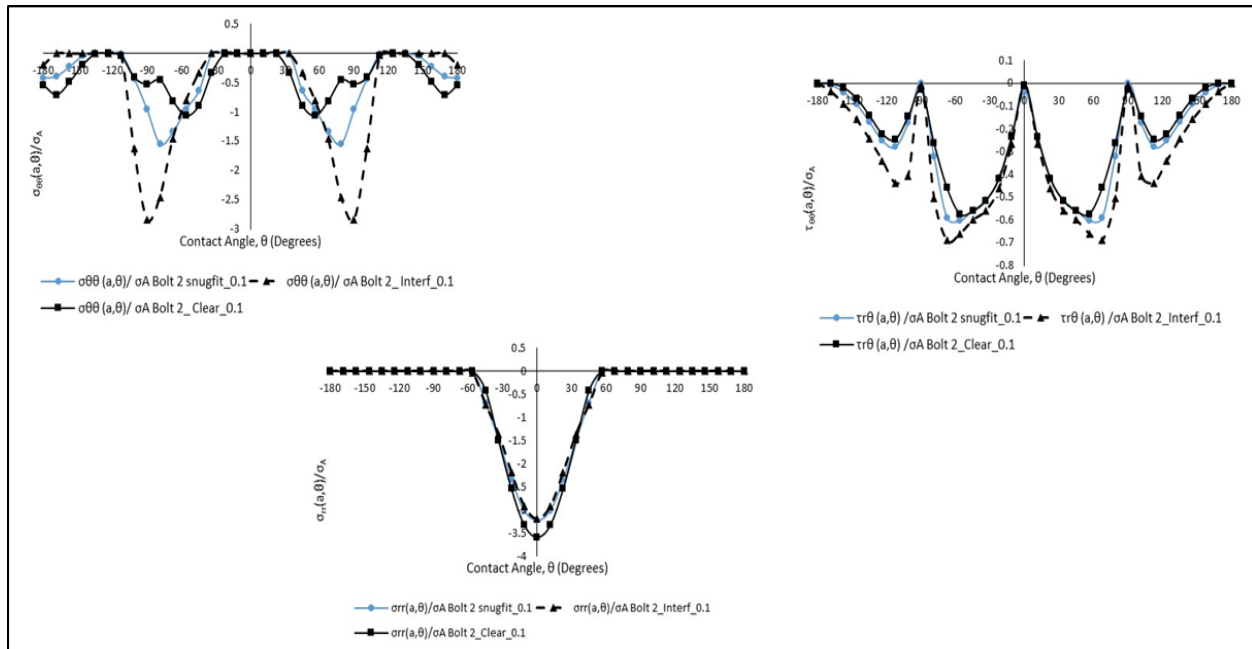
Figure 42: Effect of snug, interference and clearance fits on tangential, radial and shear contact stresses in a double lap butt joint of GFRP laminates with AA 6061-T4 butt straps for a quasi-isotropic layup in the presence of bearing and bypass loading along the boundary of the pin-loaded hole (Bolt 2: Torque = 2.2 N-m, μ= 0.1, Thickness = 5.672 mm)
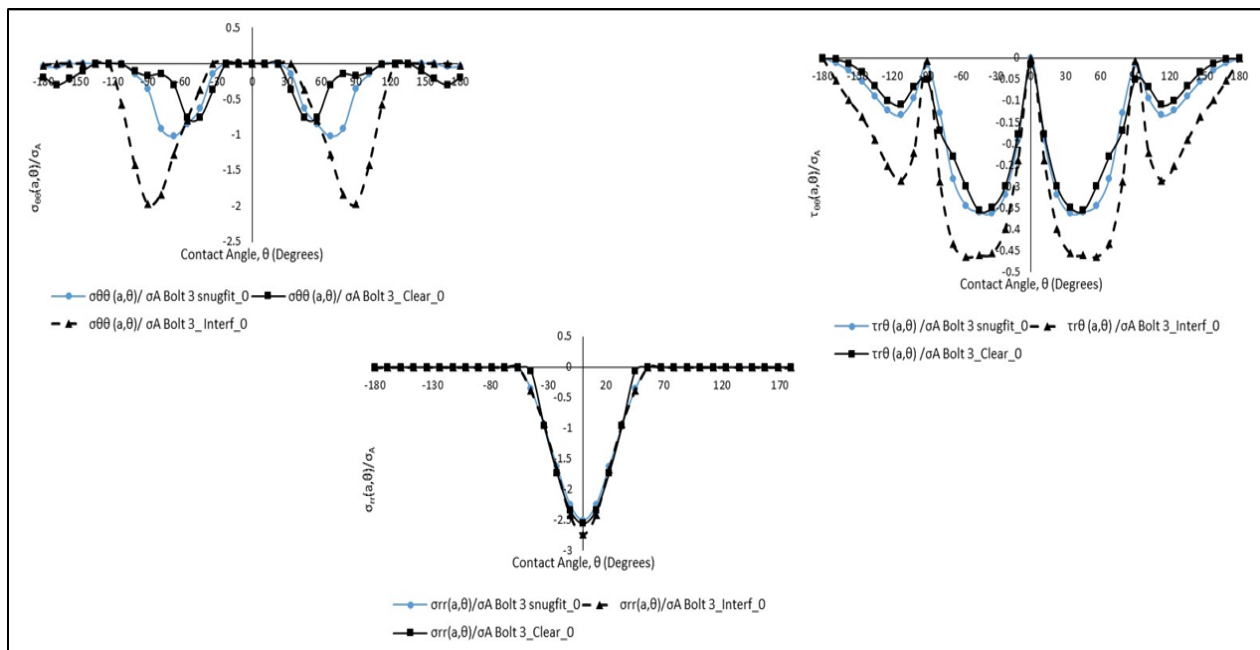

Figure 43: Effect of snug, interference and clearance fits on tangential, radial and shear contact stresses in a double lap butt joint of GFRP laminates with AA 6061-T4 butt straps for a quasi-isotropic layup in the presence of bearing and bypass loading along the boundary of the pin-loaded hole (Bolt 3: Torque = 2.2 N-m, μ= 0.0, Thickness = 5.672 mm)
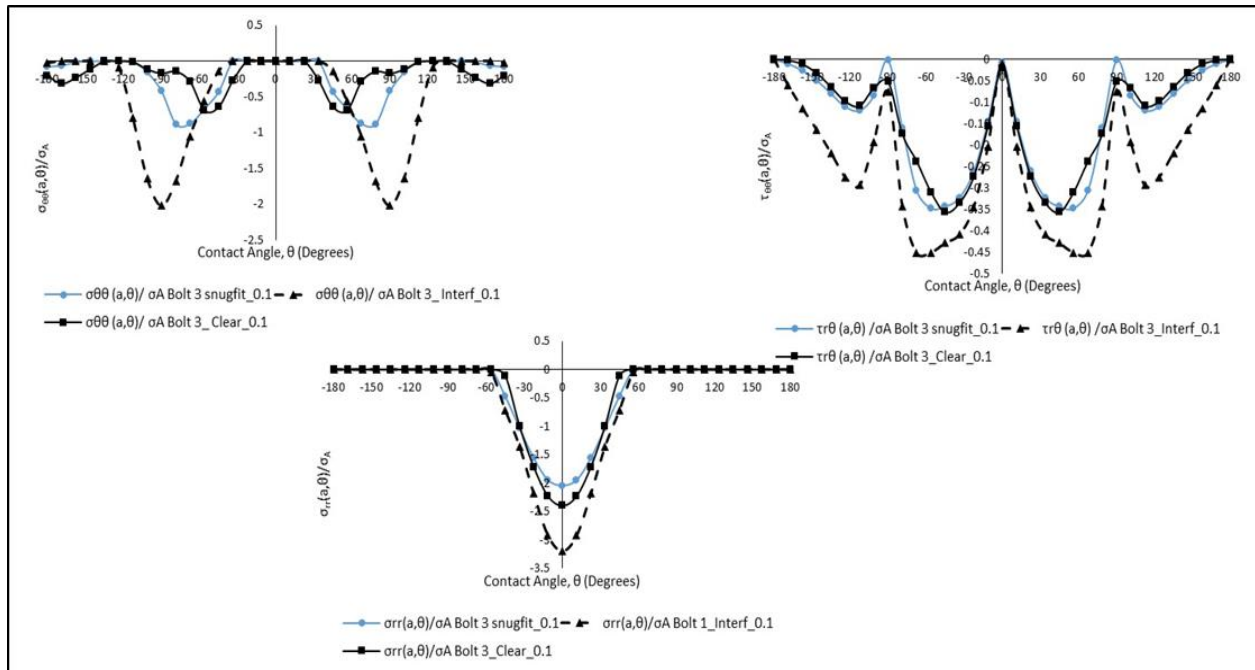
Figure 44: Effect of snug, interference and clearance fits on tangential, radial and shear contact stresses in a double lap butt joint of GFRP laminates with AA 6061-T4 butt straps for a quasi-isotropic layup in the presence of bearing and bypass loading along the boundary of the pin-loaded hole (Bolt 3: Torque = 2.2 N-m, μ= 0.1, Thickness = 5.672 mm)
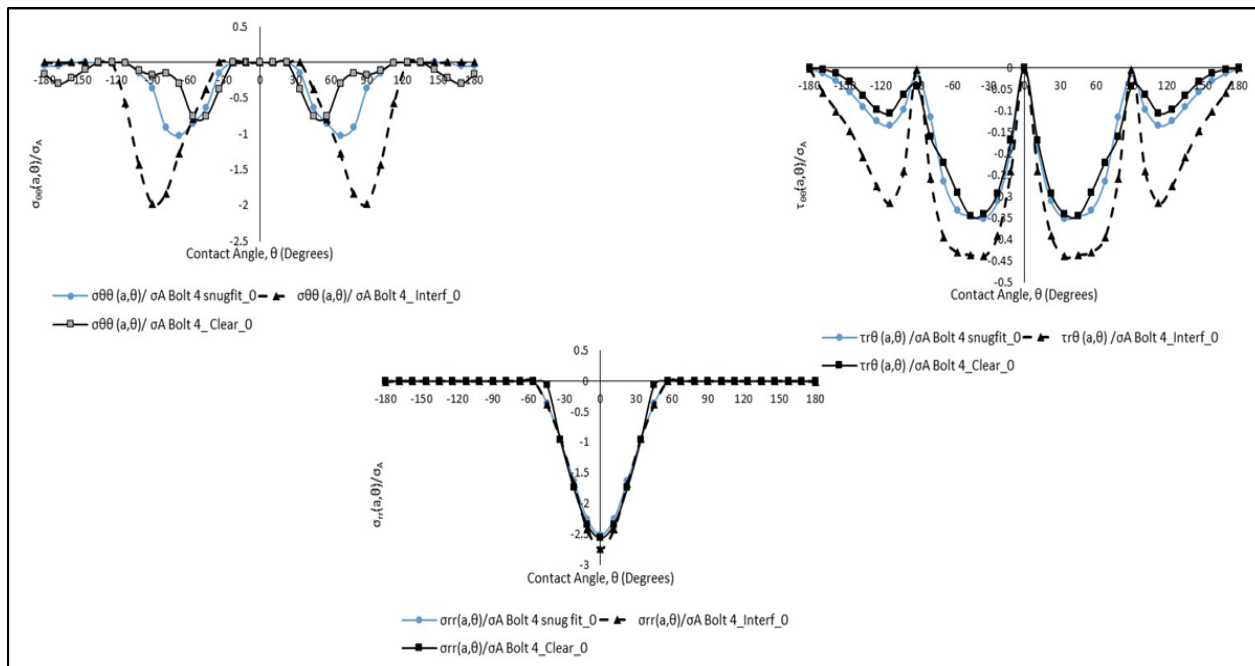

Figure 45: Effect of snug, interference and clearance fits on tangential, radial and shear contact stresses in a double lap butt joint of GFRP laminates with AA 6061-T4 butt straps for a quasi-isotropic layup in the presence of bearing and bypass loading along the boundary of the pin-loaded hole (Bolt 4: Torque = 2.2 N-m, μ= 0.0, Thickness = 5.672 mm)
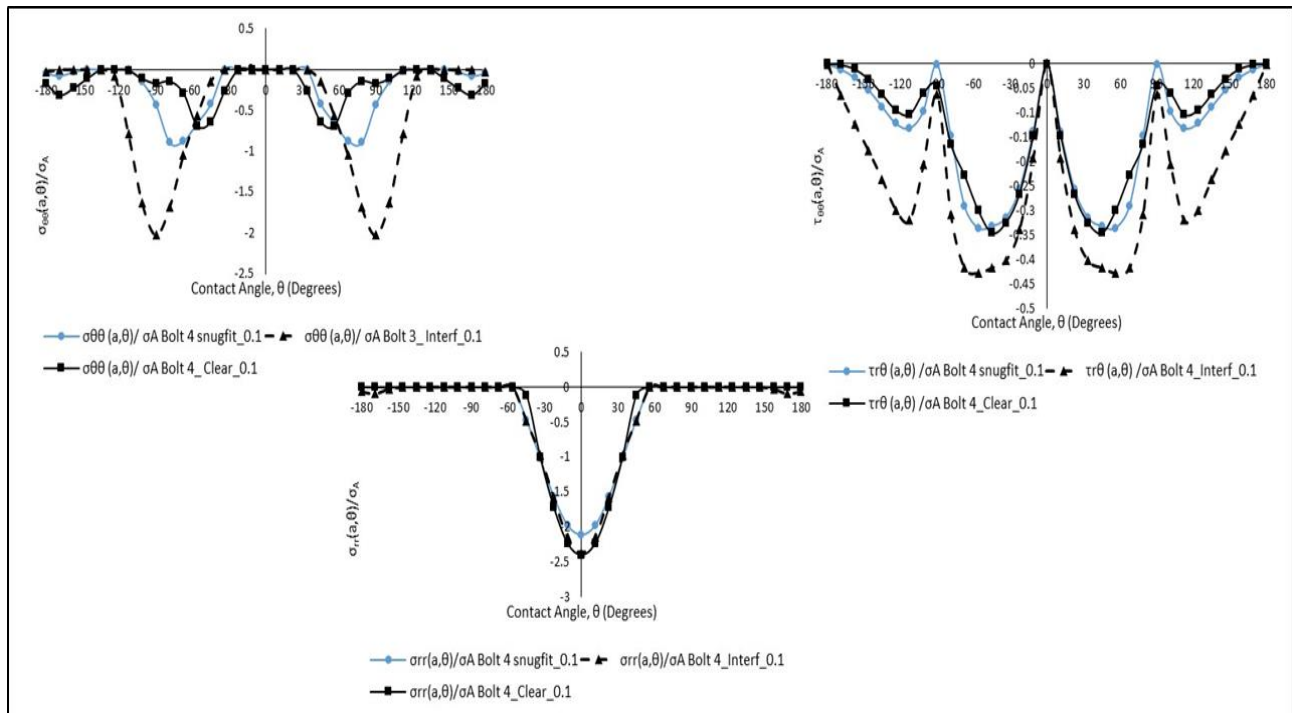
Figure 46: Effect of snug, interference and clearance fits on tangential, radial and shear contact stresses in a double lap butt joint of GFRP laminates with AA 6061-T4 butt straps for a quasi-isotropic layup in the presence of bearing and bypass loading along the boundary of the pin-loaded hole (Bolt 4: Torque = 2.2 N-m, μ= 0.1, Thickness = 5.672 mm)

4.8. Study of Pin Bearing Hole Deformation

Following the procedure suggested by [34] the real pin bearing hole deformation is separated from the measured deformation. Coefficient of friction is 0.0 and snug fit conditions for the bolt are assumed in the finite element analysis. It is observed that FEA predicts bearing hole real deformation accurately. The results are shown in Table 8. The axial displacement of different specimens is shown in Figure 47. Figures 48, to 50 show the finite element displacement results for the coupon. The bearing stress determined from the present study is compared with the results available in the literature in Figure 51 for various (w/d) ratios of specimens.

Corrected hole deformation   is defined as

$$\delta_{corrected} = \delta_L - \frac{\sigma * (L - \frac{D}{2} - X)}{E_x} \tag{12}$$

Separation of Pin Bearing Hole Deformation
The bolt is at a fixed position and the tensile load is applied at the other end of the specimen. For the section of the coupon at X = 0, Figure 2 shows the bolt hole contact point (X=0, Y=0) does not move in the analysis. However, at the same section, the coupon's lateral edge (X=0, Y=36) move 1.66 mm in the direction of the applied load (T3D6E3W6 specimens, 1.71 mm for T4D6E3W6 specimens 1.827 mm for T5D6E3W6 specimens). The discontinuous lines for the X = 3 mm

section correspond to the hole center. The section at X = 3 mm corresponds to the hole end. The hole end (X = 6, Y = 0) is therefore displaced by 1.6565 mm. This displacement corresponds to the deformation the bearing hole in the direction of the bearing load. The failure loads, ultimate stresses and the extension of the different specimens are shown in Table 9.

Table 8: Comparison of pin bearing hole deformation from experiments and finite element analysis

Deflection (mm)	T3D6E3W6	T4D6E3W6	T5D6E3W6
δ_1_FEA	1.66	1.71	1.83
δ_1_Exp	1.70	1.90	2.00
δ_1_Exp_Corr	1.66	1.71	1.84
δ_1_Exp_Corr) - δ_1_Exp, %	-2.54	-9.34	-7.98
δ_1_Exp_Corr) - δ_1_FEA, %	0.10	0.44	0.57

Table 9: Failure loads, ultimate stresses and axial extensions of specimens

| Specimen ID	Specimen Thickness, mm	Failure Load, P (N)	Average Strength, (P/Gross width*Thickness),Mpa	Specimen Extension, mm
T3D6E3W6	3.328	57820.11	237.94	2.9
T4D6E3W6	4.500	73549.13	223.85	3.6
T5D6E3W6	5.672	95036.84	229.26	4.0
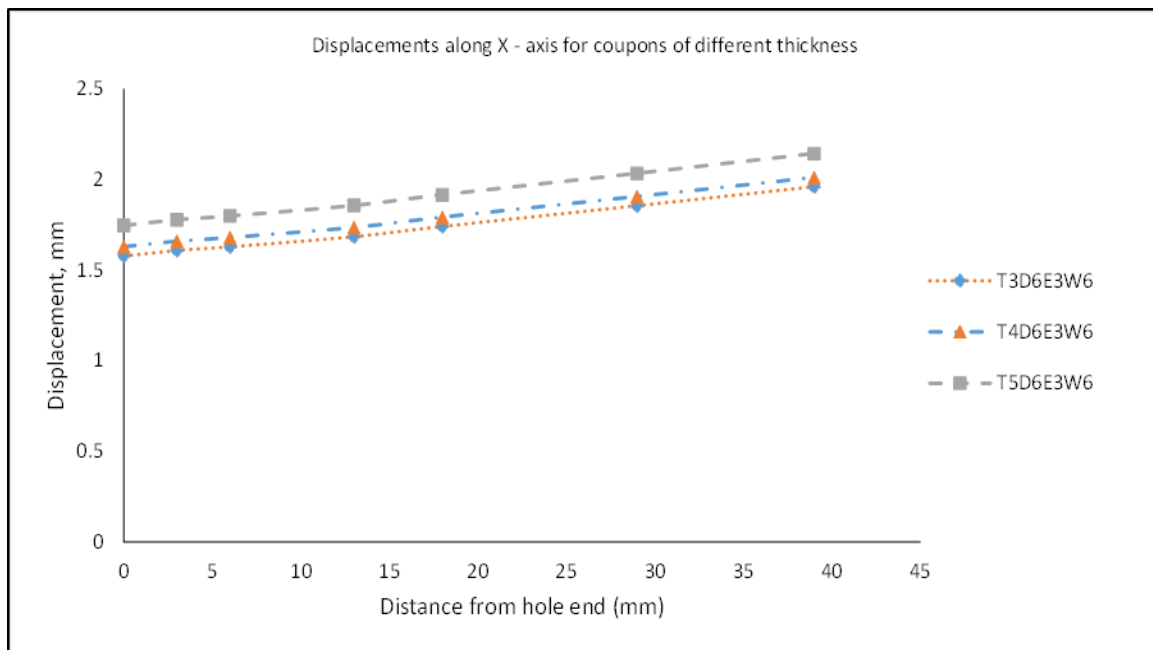
Figure 47: Finite element analysis displacement for different specimen thickness
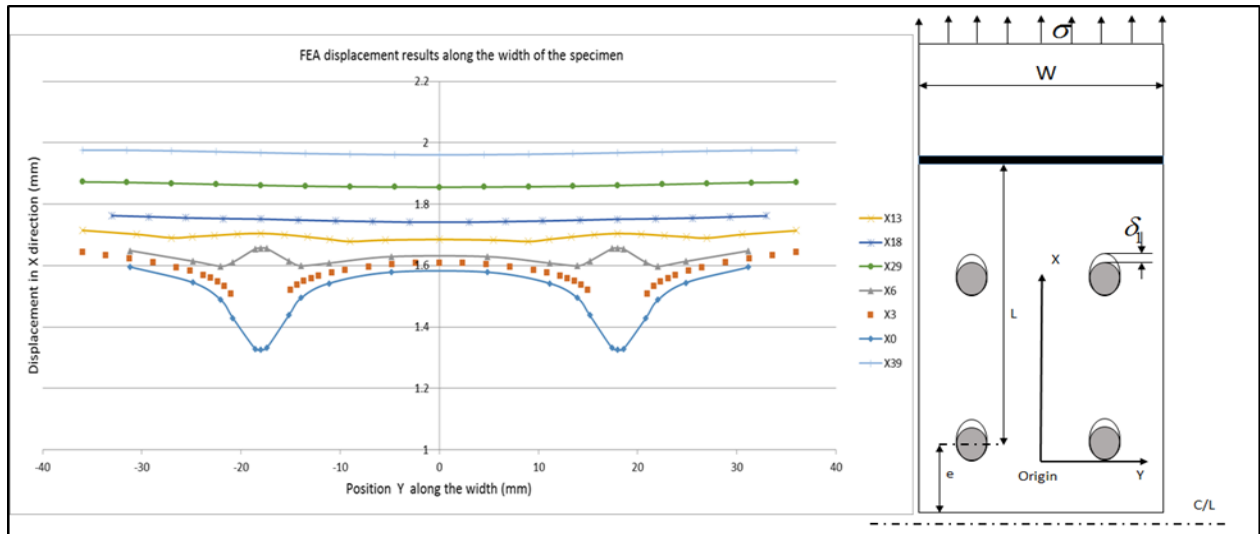
Figure 48: Finite element analysis displacement results at varying distance from origin (T3D6E3W6)
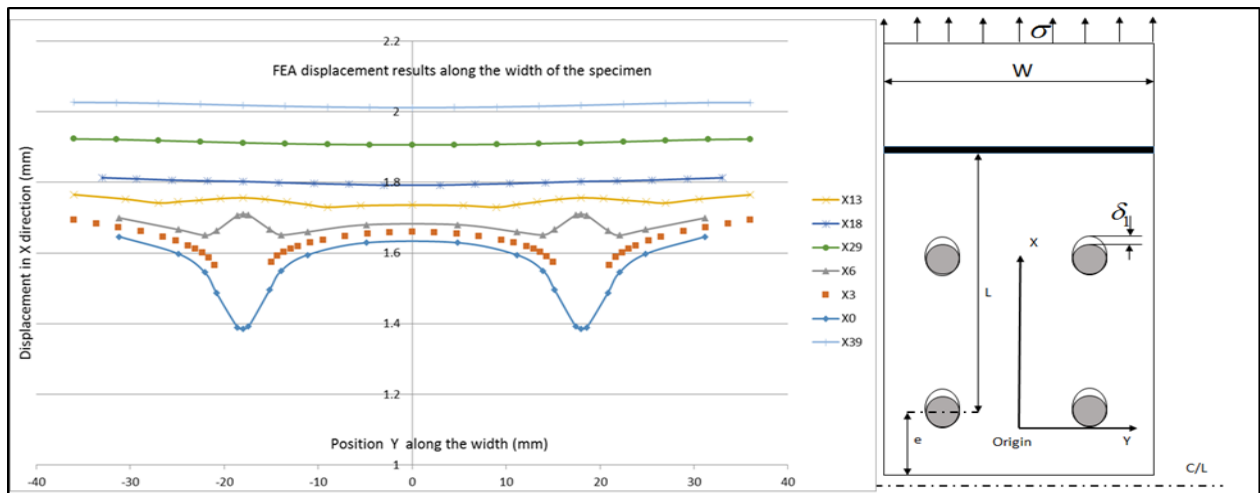

Figure 49: Finite element analysis displacement results at varying distance from origin (T4D6E3W6)
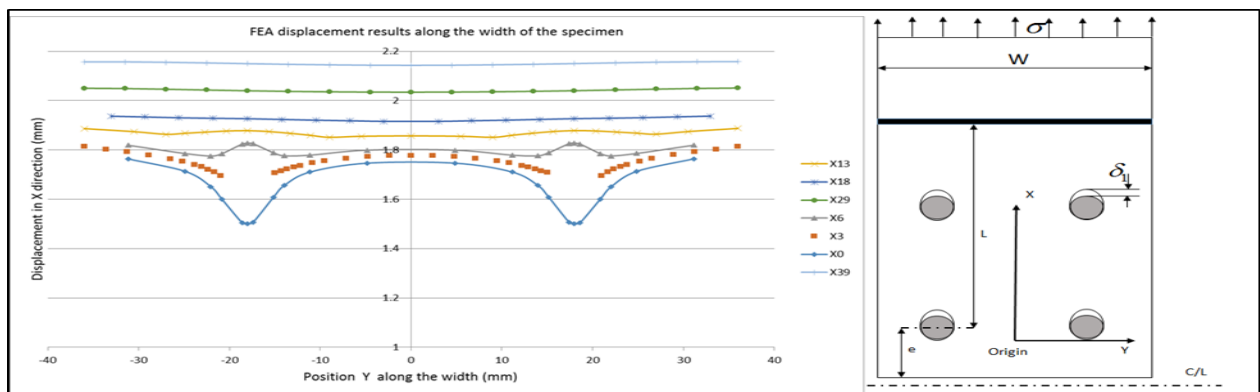

Figure 50: Finite element analysis displacement results at varying distance from origin (T5D6E3W6)
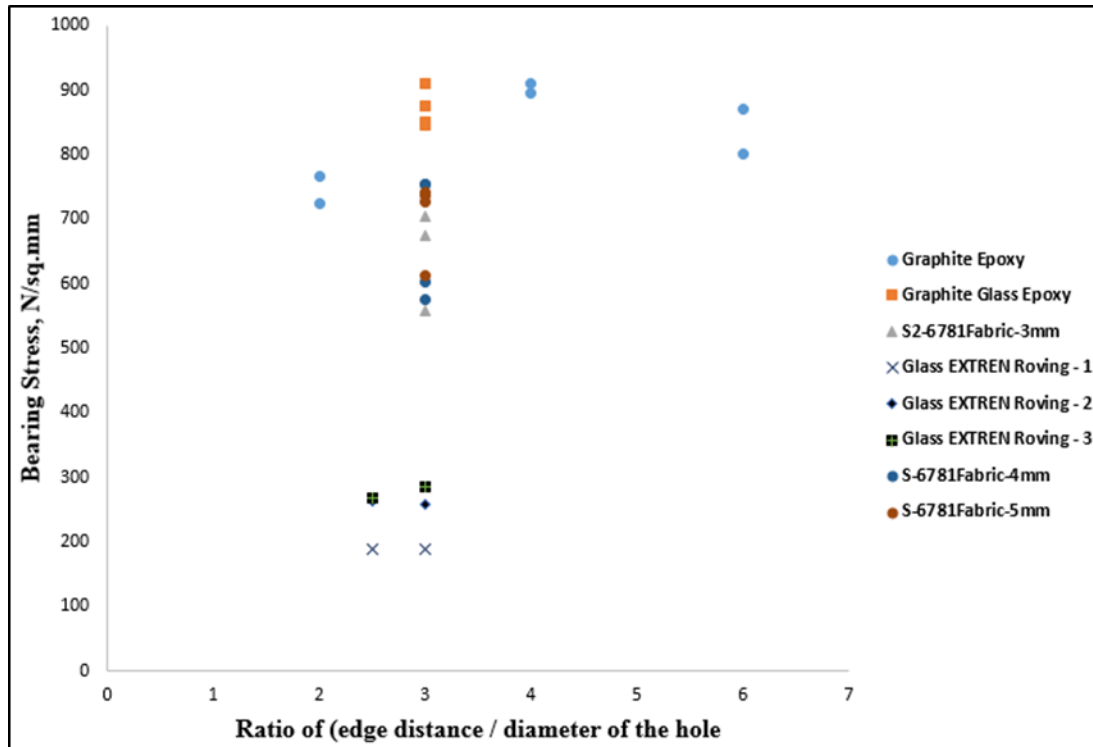
Figure 51: Comparison of bearing stress of present study with literature

4.9. Study of Stress Concentration Factors at The Bolt Holes

Stress concentration factors have a degrading effect on the fatigue life of composite joints. In metallic structures this effect has been well recognized and it's effect has been well incorporated into the methods predicting the fatigue life of the components. But, in composite structures, the stress concentration effects are more complicated and are under study stage. The holes are subjected to the effects of delamination matrix cracking, fiber breakage and failure, debonding and a combination of these failure. These can lead to net section failure, bearing failure or shear out failure. In this paper, stress concentration factors are calculated at the bolt holes using the finite element analysis for different values of (d/w) and (e/d) ratios. Laminates are treated as quasi-isotropic with equivalent elastic properties (homogenized). The results are compared with those available in the literature [35].

The gross stress concentration factor is expressed as [36]

$$\frac{K_{t\infty}}{K_{tg}} = \frac{\lambda^2}{(1-\lambda)^2} + \frac{(1-2\lambda)}{(1-\lambda)^2}\sqrt{1+(\lambda^2-1)(2a/H)^2} - \frac{\lambda^2(2a/H)^2}{(1-\lambda)\sqrt{1+(\lambda^2-1)(2a/H)^2}} + \frac{\lambda^7}{2}\left(\frac{2a}{H}\right)^6$$

$$\left(K_{t\infty} - 1 - \frac{2}{\lambda}\right)\left\{\left[1+(\lambda^2-1)\left(\frac{2a}{H}\right)^2\right]^{(-5/2)} - \left(\frac{2a}{H}\right)^2\left[1+(\lambda^2-1)\left(\frac{2a}{H}\right)^2\right]^{(-7/2)}\right\}$$

(13)

For a laminate panel,

$$K_{t\infty} = 1 + \left(\frac{1}{\lambda}\right)\sqrt{\left(\frac{2}{A_{66}}\right)}\left(\sqrt{A_{11}A_{22}} - A_{12} + \frac{A_{11}A_{22} - A_{12}^2}{2A_{66}}\right) \tag{14}$$

In terms of laminate material constants (14) is rewritten as

$$K_{t\infty} = 1 + \left(\frac{1}{\lambda}\right)\sqrt{2\left(\sqrt{\frac{E_x}{E_y}} - \upsilon_{xy} + \frac{E_x}{2G_{xy}}\right)} \tag{15}$$

Approximate Ktn is calculated from the relationship between the net and gross stress concentration factors as

The results are presented in the form of stress concentration factors for circumferential and radial stresses and normalized with respect to the applied tensile stress. The variation of stress concentration factors with respect to the circumferential stress for the three types of specimens (T3D6E3W6, T4D6E3W6 and T5D6E3W6) are shown in Figure 52 to 54 and those with radial stress are shown in Figures 55 to 57.
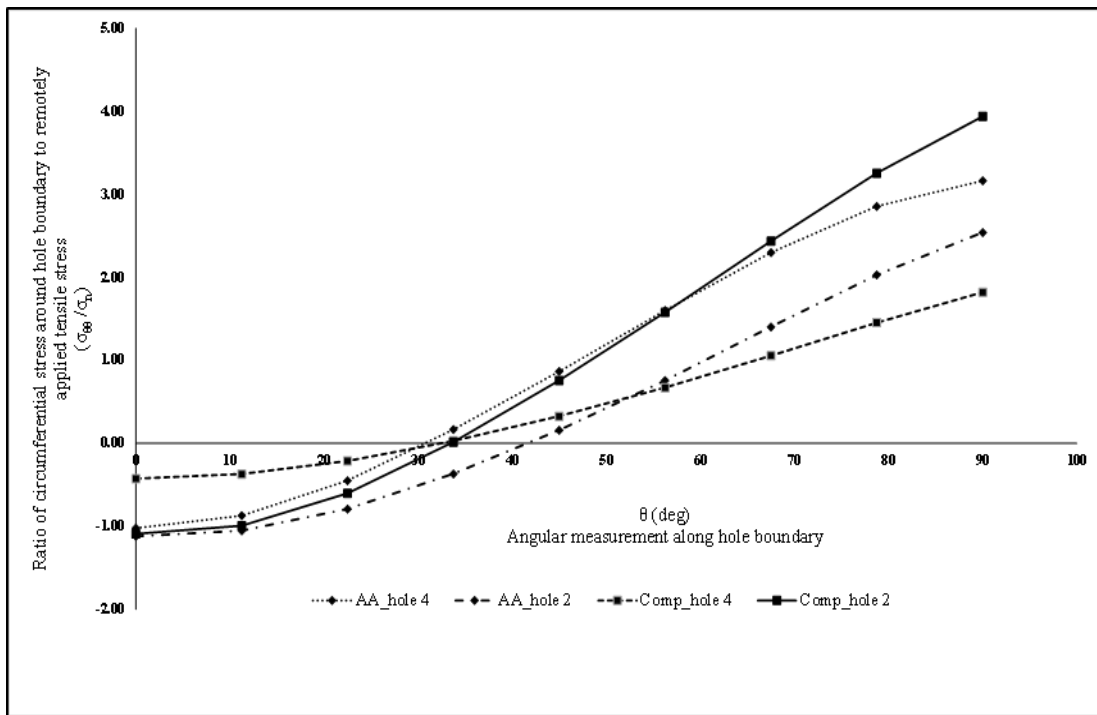

Figure 52: Stress concentration factors for circumferential stress with snug fit in a double lap butt joint of GFRP laminates with AA 6061-T4 butt straps for a quasi-isotropic layup in the presence of bearing and bypass loading along the boundary of the pin-loaded hole (Bolt 2 and 4, (w/d) = 6, (e/d) = 3, Torque = 0.0 N-m, μ= 0.0, Thickness = 3.326 mm)
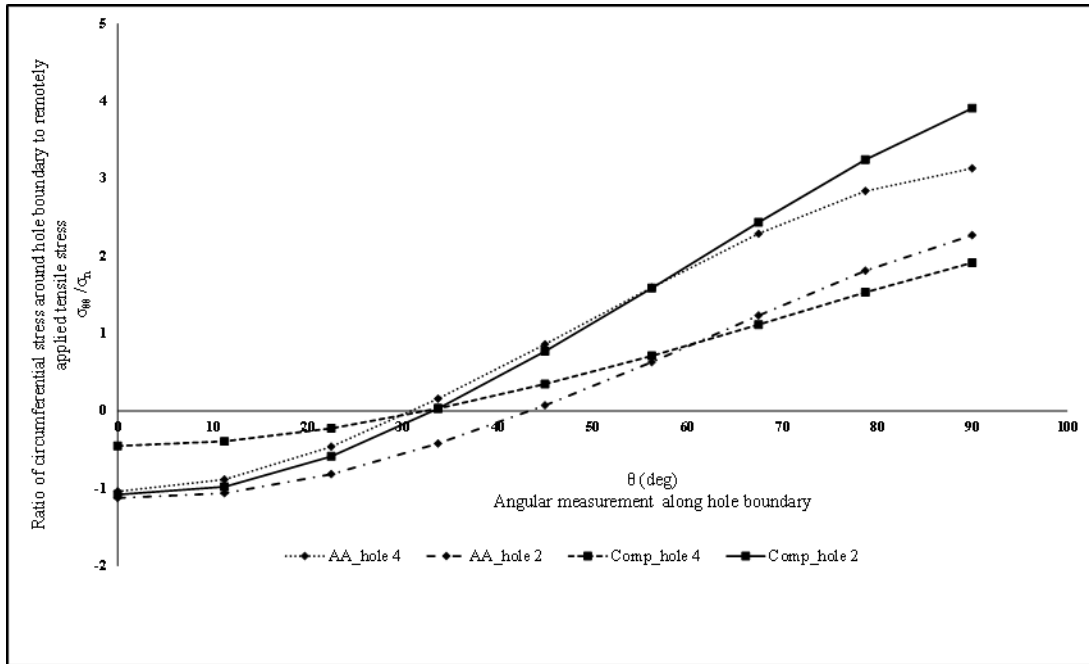
Figure 53: Stress concentration factors for circumferential stress with snug fit in a double lap butt joint of GFRP laminates with AA 6061-T4 butt straps for a quasi-isotropic layup in the presence of bearing and bypass loading along the boundary of the pin-loaded hole (Bolt 2 and 4, (w/d) = 6, (e/d) = 3, Torque = 0.0 N-m, μ= 0.0, Thickness = 4.5 mm)
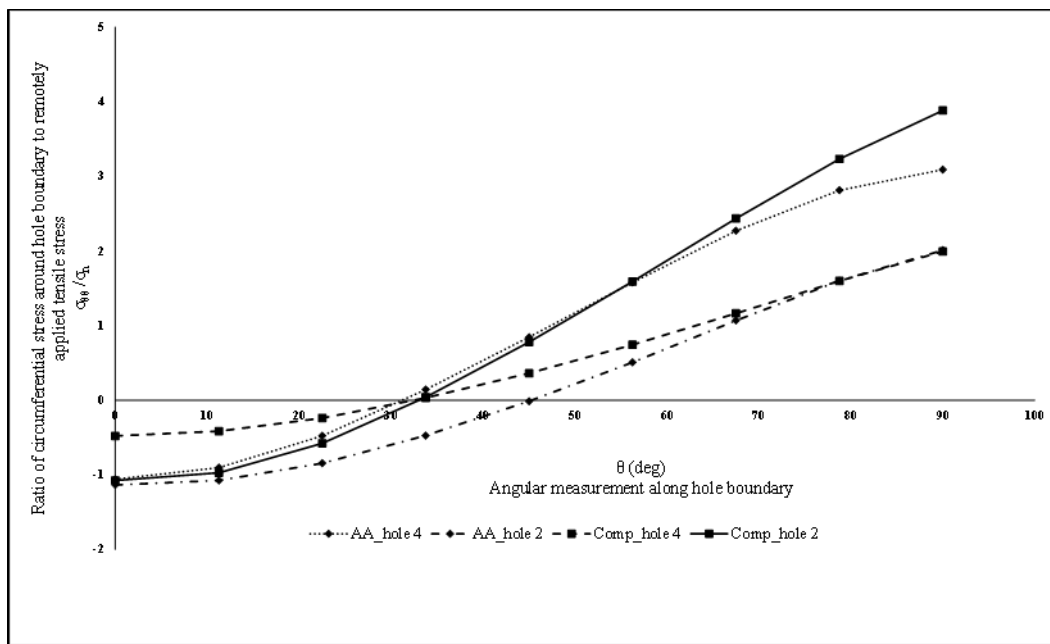

Figure 54: Stress concentration factors for circumferential stress with snug fit in a double lap butt joint of GFRP laminates with AA 6061-T4 butt straps for a quasi-isotropic layup in the presence of bearing and bypass loading along the boundary of the pin-loaded hole (Bolt 2 and 4, (w/d) = 6, (e/d) = 3: Torque = 0.0 N-m, μ= 0.0, Thickness = 5.672 mm)
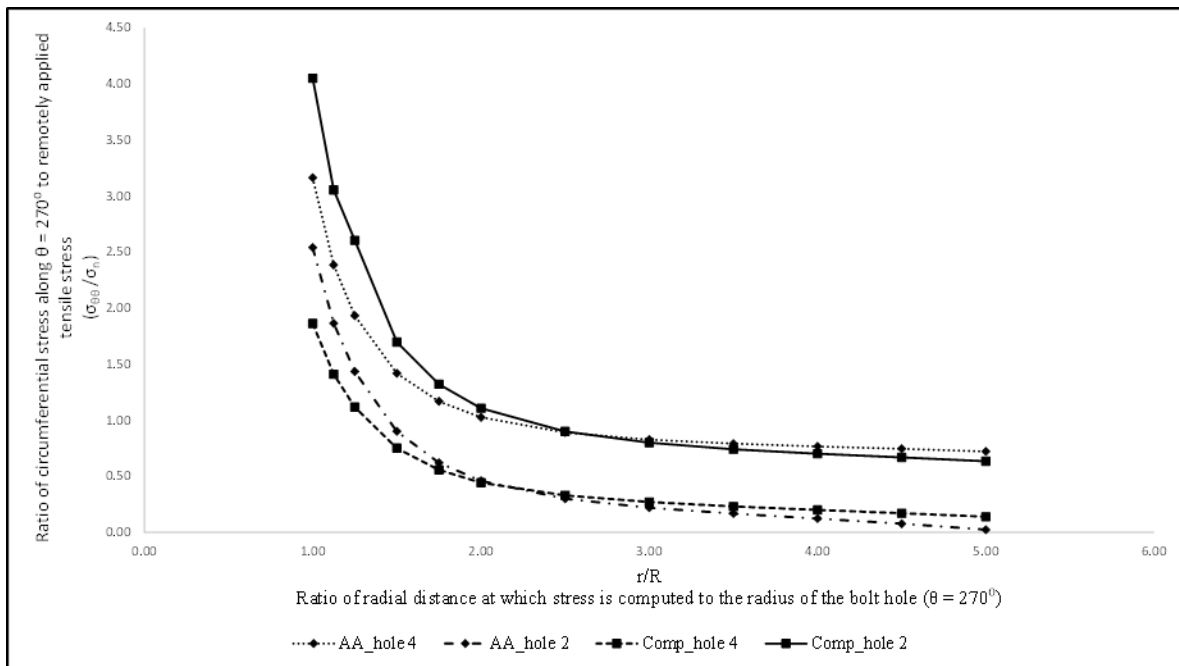
Figure 55: Stress concentration factors for circumferential stress with snug fit in a double lap butt joint of GFRP laminates with AA 6061-T4 butt straps for a quasi-isotropic layup in the presence of bearing and bypass loading along the boundary of the pin-loaded hole (Bolt 2 and 4, (w/d) = 6, (e/d) = 3: Torque = 0.0 N-m, μ= 0.0, Thickness = 3.326 mm)
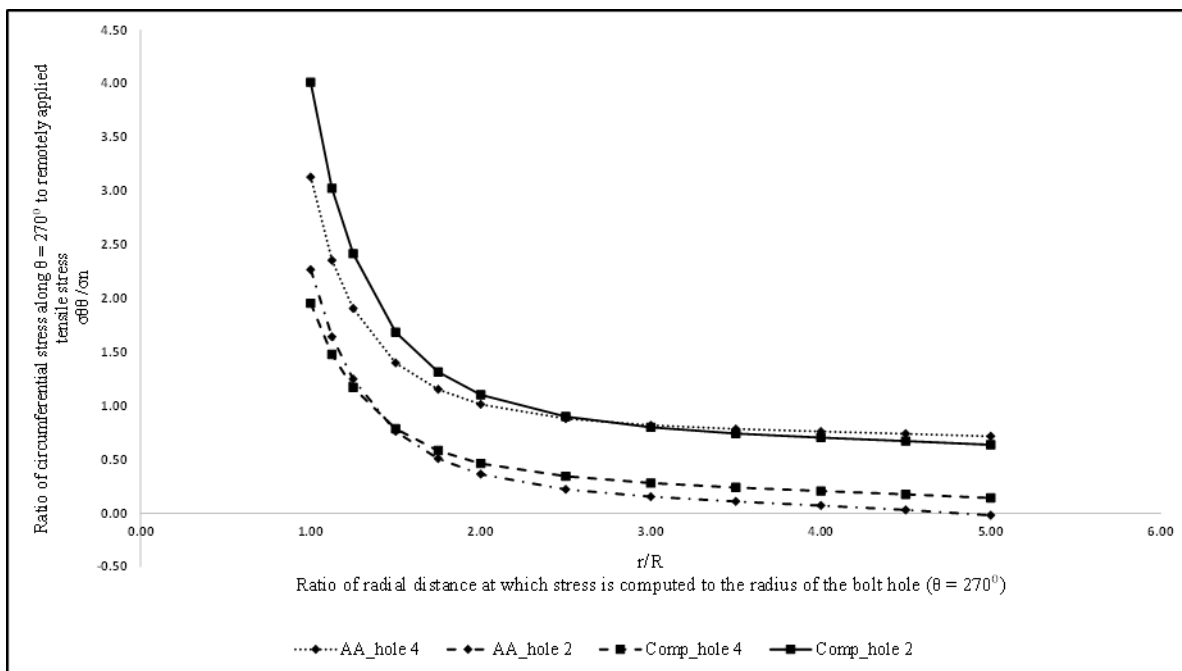

Figure 57: Stress concentration factors for circumferential stress with snug fit in a double lap butt joint of GFRP laminates with AA 6061-T4 butt straps for a quasi-isotropic layup in the presence of bearing and bypass loading along the boundary of the pin-loaded hole (Bolt 2 and 4, (w/d) = 6, (e/d) = 3: Torque = 0.0 N-m, μ= 0.0, Thickness = 4.5 mm)
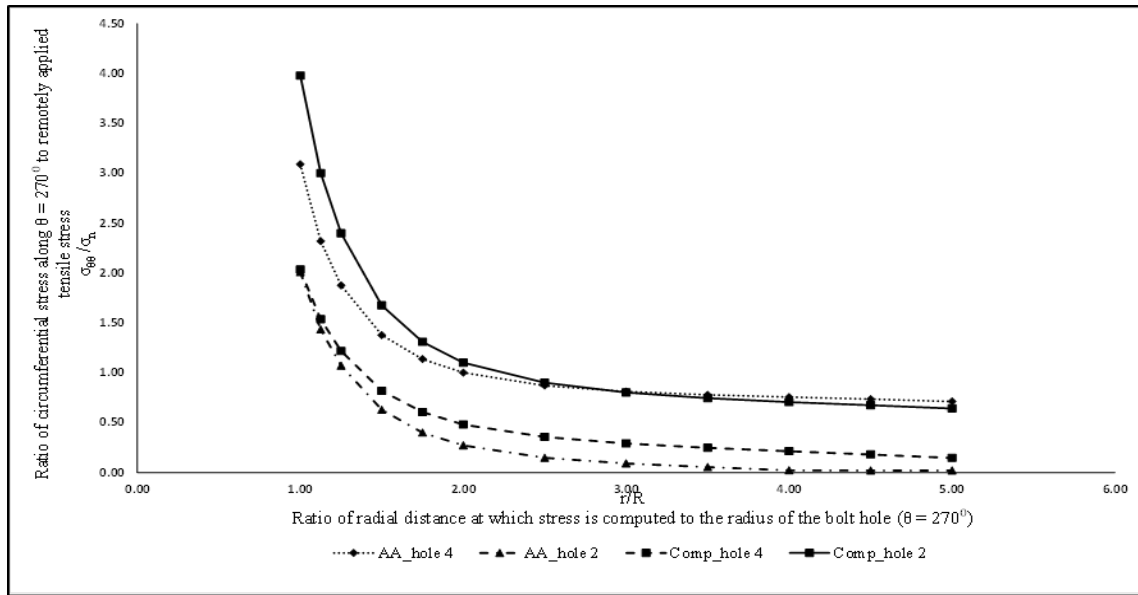
Figure 56: Stress concentration factors for circumferential stress with snug fit in a double lap butt joint of GFRP laminates with AA 6061-T4 butt straps for a quasi-isotropic layup in the presence of bearing and bypass loading along the boundary of the pin-loaded hole (Bolt 2 and 4, (w/d) = 6, (e/d) = 3: Torque = 0.0 N-m, μ= 0.0, Thickness = 5.672 mm)

4.10. Study of Effect of Change in Butt Strap Thickness

The butt strap thickness was changed from 5 mm to 4 mm to study the change in the von Mises stress. The stress plots are shown in Figure 57 and 58. It is observed that the top and bottom butt straps have different distribution. This is attributed to the difference in the type of contact at the head (standard contact) and nut side (bonded contact) of the bolt.
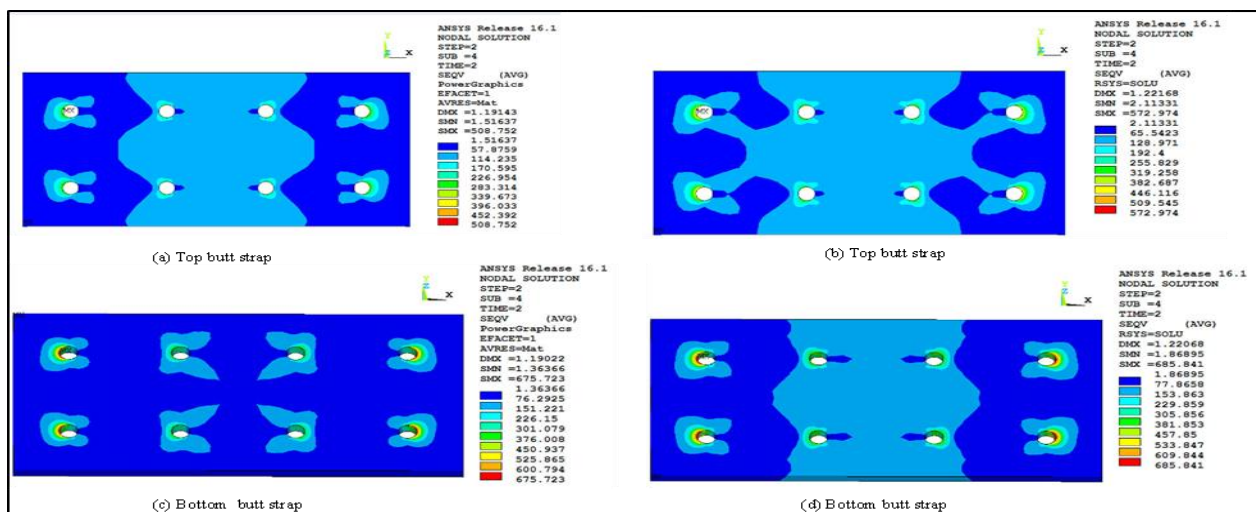
Figure 57: Effect of thickness of butt strap on von Mises stress in butt strap of a double lap butt joint of GFRP laminates with AA 6061-T4 butt straps for a quasi-isotropic layup in the presence of bearing and bypass loading (Torque = 2.2 N-m, μ= 0.0, Thickness = 3.326 mm, Snug Fit): (a). Tbutt strap = 5 mm, (b). Tbutt strap = 4 mm, (c). Tbutt strap = 5 mm, (d). Tbutt strap = 4 mm

(a) Top butt strap

(b) Top butt strap

(c) Bottom butt strap

(d) Bottom butt strap
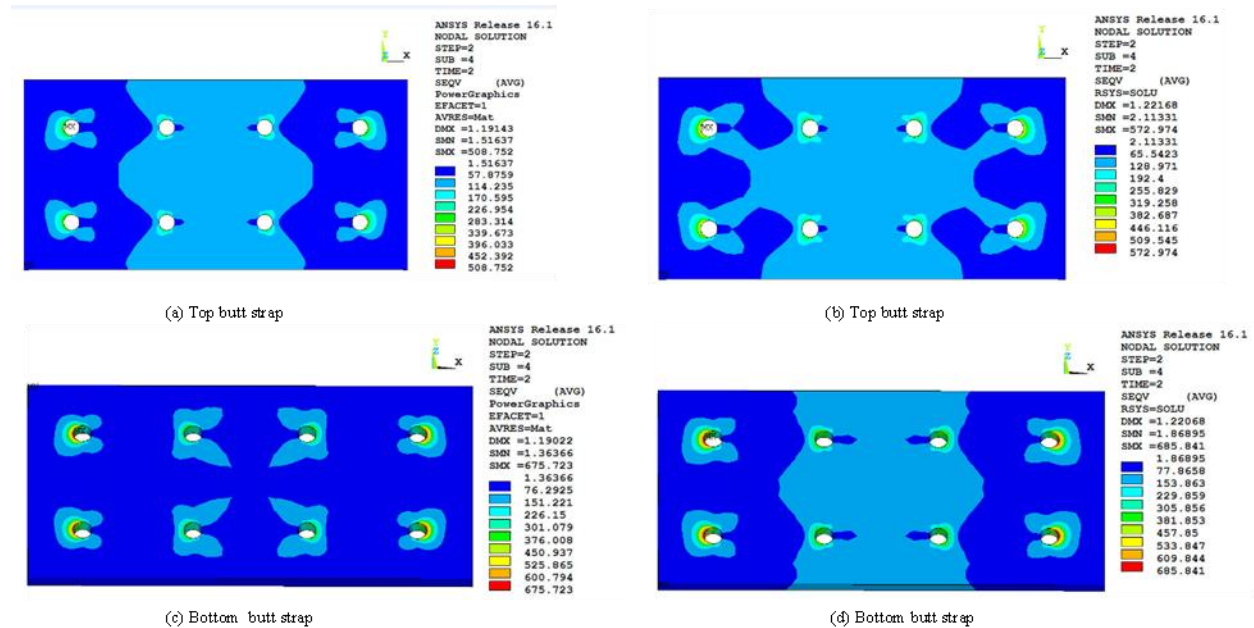
Figure 58: The effect of thickness of butt strap on von Mises stress in butt strap of a double lap butt joint of GFRP laminates with AA 6061-T4 butt straps for a quasi-isotropic layup in the presence of bearing and bypass loading (Torque = 2.2 N-m, μ= 0.0, Thickness = 3.326 mm, Interference Fit): (a). Tbutt strap = 5 mm, (b). Tbutt strap = 4 mm, (c). Tbutt strap = 5 mm, (d). Tbutt strap = 4 mm

5. Conclusions

Comprehensive study of an eight bolted composite laminate butt joint with aluminum alloy butt straps is presented. It is concluded that the fabrication process used is consistent because it produced different specimens having comparable fiber volume fraction and laminate elastic properties. The behaviour of the joint in handling the bearing bypass loads at the onset of damage corresponding to the first ply failure is presented. This study clearly predicts the net tension failure after the bearing failure at the bolt holes. The nonlinear behaviour of the specimens is evident in the test plot of load versus displacement. This nonlinear behaviour is possibly due to varying contact arc between the bolt and the specimen during the loading process. In the study of load distribution among the four bolts, it is observed that the loads are not equally distributed between the bolts. This is attributed to the possible difference in the fits between the different bolts. It is also concluded that the load distribution among the four bolts predicted on the assumption that it is proportional to the maximum ordinate of the bearing mark at each bolt is reasonably accurate. It is further concluded that the last rows of bolts closer to the loading edge or grip carry higher load when compared to the inner row (this is in agreement with the earlier well established observation). It is shown that in this joint the bolt hole axial deformation is different at different bolt hole and hence the stiffness (effect of material anisotropy) of the laminate is different at different locations. It is concluded that the friction doesn't affect the bolt hole deformation in the specimens of different thickness. The comparison of bolt hole deformation between finite element analysis and test is good within the limits of measurement error for three types of fit. It is seen that the circumferential and shear contact stresses are affected in the three types of fit; while radial contact stress is affected to a less degree among the four bolts. The hole deformation due to pin

bearing load is shows very small correction in the specimens deformation. Stress concentration factors in butt plates are less than those in composite laminate plates.

Acknowledgement

References

[1]   Hart-Smith L. J, Bolted Joints in Graphite Epoxy Composites, 1976, NASA Contractor Report, NASA CR-144899

[2]   Fu-Kuo Chang and George S. Springer, Richard A. Scott, Bolted joints in laminated composites, 1984, American Institute of Aeronautics and Astronautics, Inc.

[3]   Fu-Kuo Chang and Richard A. Scott, George S. Springer, Failure of Composite Laminates Containing Pin Loaded Holes – Method of Solution, 1984, Journal of Composite Materials, Vol. 18.

[4]   Madenci E., Ileri L., Analytical of pin-loaded holes in composite laminates under combined bearing-bypass and shear loading, 1995, International Journal of Solids Structures, Vol. 32, No. 14, pp. 2053 – 2062.

[5]   Yang B., Pan E. Yuan F.G., Three dimensional stress analysis in composite laminates with an elastically pinned hole, 2003, International Journal of Solids Structures, 40 (2003), pp. 2017 – 2035.

[6]   Crews J.H., Naik R.A., Combined bearing and bypass loading on a graphite/epoxy laminate, 1986, Composite Structures 6 (1986) 21 – 40.

[7]   H.A. Whitworth, O. Aluko, N.A. Tomlinson, Application of the point stress criterion to the failure of composite pinned joints, 2008, Engineering Fracture Mechanics 75 (2008) pp 1829–1839.

[8]   Olanrewaju Aluko, An Analytical Method for Failure Prediction of Composite Pinned Joints, 2011, Proceedings of the World Congress on Engineering 2011 Vol III WCE 2011, July 6 - 8, 2011, London, U.K.

[9]   Álvaro Olmedo, Carlos Santiuste, On the prediction of bolted single-lap composite joints, 2012, Composite Structures 94 (2012) 2110–2117.

[10] M. M. Moure S. Sanchez-Saez, E. Barbero, E. J. Barbero, Analysis of damage localization in composite laminates using a discrete damage model, 2014, Composites Part B: Engineering 66: 224-232.

[11] Iqbal Shahid, Fu-Kuo Chang, An accumulative damage model for tensile and shear failures of laminated composite plates, 1995, Journal of Composite Materials, Vol. 29, No. 7.

[12] Zlatan Kapidžić, Larsgunnar Nilsson, Hans Ansell, Finite element modeling of mechanically fastened composite-aluminum joints in aircraft structures, 2014, Composite Structures 109 (2014) pp 198–210.

[13] Karami G., Sharifi - Jah M. R., Failure analysis of laminated composite pinned connections, 1999, Scientia Iranica Vol. 6 No. 2 pp 86 – 100.

[14] M. S. Meon, M. N. Rao, K-U. Schr̈oder, Numerical Prediction of Bearing Strength on Composite Bolted Joint Using Three Dimensional Puck Failure Criteria, 2016, World Academy of Science, Engineering and Technology International Journal of Chemical, Molecular, Nuclear, Materials and Metallurgical Engineering Vol:10, No:10, 2016.

[15] F. Rosales-Iriarte, N.A. Fellows, J.F. Durodola, Experimental evaluation of the effect of clamping force and hole clearance on carbon composites subjected to bearing versus bypass loading, 2011, Composite Structures 93 (2011) 1096 – 1102.

[16] Binnur Gören Kiral, Effect of the clearance and interference-fit on failure of the pin-loaded composites, 2010, Materials and Design 31 (2010) 85–93.

[17] P.J. Gray, R.M. O'Higgins, C.T. McCarthy, Effects of laminate thickness, tapering and missing fasteners on the mechanical behaviour of single-lap, multi-bolt, countersunk composite joints, 2014, Composite Structures 107 (2014) pp 219–230.

[18] Ivana Ilić – Zlatko Petrovic – Mirko Maksimović – Slobodan Stupar – Dragi Stamenković, Computation Method in Failure Analysis of Mechanically Fastened Joints at Layered Composites, 2011, Strojniški vestnik - Journal of Mechanical Engineering 58(2012)9, pp 553-559.

[19] Srinivasa D. Thoppul, Joana Finegan, Ronald F. Gibson, Mechanics of mechanically fastened joints in polymer–matrix composite structures – A review, 2009, Composites Science and Technology 69 (2009) pp 301–329.

[20] P. P. Camanho and F. L. Matthews, Stress analysis and strength prediction of mechanically fastened joints in FRP: a review, 1997, Composites Part A 28A, Elsevier Science Limited, pp 529 – 547.

[21] Yi Xiao, Takashi Ishikawa, Bearing strength and failure behavior of bolted composite joints (part I: Experimental investigation), 2005, Composites Science and Technology 65 (2005) pp 1022–1031.

[22] Fengrui Liu, Libin Zhao, Saqib Mehmood, Jianyu Zhang, Binjun Fei, A modified failure envelope method for failure prediction of multi-bolt composite joints, 2013, Composites Science and Technology 83 (2013) pp 54–63.

[23] P.P. Camanho, M. Lambert, A design methodology for mechanically fastened joints in laminated composite materials, 2006, Composites Science and Technology 66 (2006) pp 3004–3020.

[24] Pedro Ponces Camanho, Failure criteria for fibre-reinforced polymer composites, 2002, DEMEGI.

[25] Joseph Edward Shigley, Charles R. Mischke, 1989, Mechanical Engineering Design, Fifth Edition,.

[26] Michelle Man, Yeow Ng, Ed Hooper, 2013, Advanced Composites Group, ACG MTM45-1 6781 S2 glass 35% RC qualification material property data report, SP3505WI-Q, National Institute of Aviation Research (NIAR).

[27] Libin Zhao, Tianliang Qin, Jianua Zhang, Yuli Chen, 2015, 3D gradual material degradation model for progressive damage analysis of unidirectional composite materials, Mathematical problems in engineering, Volume 2015, Article Id 145629, 11 pages.

[28] Metallic Materials Properties Development and Standardization, MMPDS-07, April 2012.

[29] Unbrako Engineering Guide.

[30] Yang Xu, Zhang Yining, Xu Xiwu, A strength analysis method of composite plate with multiple bolted joints, Acta Aeronautica Et Astronautica Sinica, 1998, pp. 1998-2001.

[31] John L. Clarke, Structural Design of Polymer Composites EUROCOMP Design Code and Handbook, 1996, Chapman & Hall

[32] Autar K. Kaw, Mechanics of Composite Materials, Second Edition, 2006, pages 342 – 360

[33] Elbridge Z. Stowell, Stress and Strain Concentration at a Circular Hole in an infinite plate, NASA TN 2073, April 1950

[34] B. Vangrimde, R.Boukhili, Measuring bolted joint bearing deformation and stiffness, ICCM12, Conference Paris July 1999, Paper ID 912, ISBN2-9514526-2-4.

[35] John H. Crews Jr., C. S. Hong, I. S. Raju, Stress Concentration Factors for Finite Orthotropic Laminates with a Pin-Loaded Hole, NASA-TP-1862, May 1981

[36] Walter D. Pilkey, Deborah F. Pilkey, Peterson's Stress Concentration Factors, 3rd edition, 2008.

*Corresponding author.
E-mail address: Subramanya.Sastry@ cyient.com